Propellant Mass Scaling and Decoupling and Improved Plasma Coupling in a Pulsed Inductive Thruster

by

Taylor Raines

A Thesis Presented in Partial Fulfillment
of the Requirement for the Degree
Master of Science

Approved June 2018 by the
Graduate Supervisory Committee:

Timothy Takahashi, Chair
Daniel White
Werner Dahm

ARIZONA STATE UNIVERSITY

August 2018

ABSTRACT

Two methods of improving the life and efficiency of the Pulsed Inductive Thruster (PIT) have been investigated. The first is a trade study of available switches to determine the best device to implement in the PIT design. The second is the design of a coil to improve coupling between the accelerator coil and the plasma. Experiments were done with both permanent and electromagnets to investigate the feasibility of implementing a modified Halbach array within the PIT to promote better plasma coupling and decrease the unused space within the thruster. This array proved to promote more complete coupling on the edges of the coil where it had been weak in previous studies. Numerical analysis was done to predict the performance of a PIT that utilized each suggested switch type. This model utilized the Alfvén velocity to determine the critical mass and energy of these theoretical thrusters.

To my eternally patient wife, Allex, who has miraculously stuck with me through the course of this project.

ACKNOWLEDGMENTS

This research was made possible by the support of those around me and the hard work done by other researchers in the field. I would like to acknowledge and thank a few individuals specifically:

My wife, Allex, who keeps me sane and happy, no matter what else is happening in the world.

My parents, Ken and Patty, who supported me in chasing all of my crazy dreams.

My grandfather, Dwight Clark, from whom I discovered the accessibility of the stars.

Daniel White, who guided me through this project and showed me just how much there is out there to learn.

Timothy Takahashi, who showed me that all knowledge gained is applicable if you're willing to use it.

Werner Dahm, who showed me really how simple the workings of the world can be if I don't over-complicate it.

C. L. Dailey, R. H. Lovberg, and Kurt A. Polzin, though they don't know who I am, I could not have done any of this without the amazing work they did and continue to do in the field of plasma acceleration.

TABLE OF CONTENTS

CHAPTER Page

CHAPTER Page

LIST OF TABLES

LIST OF FIGURES

Figure Page

Figure Page

Chapter 1

INTRODUCTION

Pulsed inductive thrusters (PITs) are unsteady electromagnetic plasma accelerators that do not require electrodes. They use energy stored in a capacitor bank that is then pulsed through an inductive coil which, in turn induces an ionizing current sheet in the propellant gas near the face of the coil. Also induced by the current in the coil is a radial magnetic field. The current sheet interacts with this magnetic field which produces a Lorentz body force that accelerates the plasma sheet. The accelerated plasma "snowplows" the downstream neutral propellant, resulting in more accelerated mass, thereby producing thrust.(33)

This unsteady mode of operation offers many advantages over other forms of electric propulsion. By operating in this unsteady mode, these thrusters can maintain a set amount of thrust across a range of power sources by adjusting the pulse rate. They do not have electrodes and thus do not suffer from life-limiting factors due to propellant contamination or erosion. One of the greatest advantages is that almost any gas can be used as a propellant. This mode of operation offers a wider range of design options for use in balancing safety, cost, and efficiency.

1.1 Propulsion

Before going any deeper into the specific design of the PIT, some background information on thrusters in general is needed. Examining the topic broadly, there are two types of propulsion systems: chemical and electric. (29)

1.1.1 Chemical Propulsion

Chemical rockets are what most people associate with space travel, converting chemical energy into jet-kinetic energy. These propulsion systems are always spectacular to see in action and capable of large amounts of thrust; however, they can only fire for short periods of time.

1.1.2 Electric Propulsion

Conversely, electric propulsion systems produce very little thrust, but they operate with incredible efficiency. They can fire continuously for long periods of time, and in doing so, they achieve a much greater increase in velocity, often referred to as ΔV. This concept can be demonstrated using eq.(1.1) and eq.(1.2).

$$\Delta V = a * \Delta t \tag{1.1}$$

$$F = m * a \tag{1.2}$$

These two equations are used to derive Tsiolkovsky's rocket equation where Isp is the specific impulse, g_0 is earth's gravity, m_0 is the initial mass of the craft, and m_f is the final mass:

$$\Delta V = Isp * g_0 * ln\Big(\frac{m_0}{m_f}\Big) \tag{1.3}$$

To put this in perspective, the first stage of the Saturn V, the rocket that put man on the moon, is capable of generating 35 MN of thrust for 168 seconds. Given its mass, this yields a total ΔV of 2.575 km/s.(4) The Hall thruster at JAXA can only produce 280 mN of thrust, but can fire continuously for nearly 36 days to produce a ΔV of 5 km/s.(12) This large ΔV is what makes electric thrusters so attractive for extra-atmospheric missions. Another benefit to these thrusters is that they can be turned on and off as need dictates throughout the mission.

Electric propulsion systems can be divided into three categories: electrothermal, electrostatic, and electromagnetic.(16) Electrothermal thrusters operate by electrically heating a gas to expand out of a nozzle, similar in function to a chemical rocket. Electrostatic thrusters create thrust by accelerating ionized particles by applying electric body forces (positive-negative charge attraction). The third classification, electromagnetic propulsion, operates by applying a magnetic field to a charged plasma. The PIT falls into this last category.

More specifically, PITs are a form of unsteady electromagnetic propulsion. As the name implies, these systems operate using a pulsed firing system as opposed to their steady counterparts which fire continuously. Unsteady systems are inherently more complicated devices and more difficult to simulate; however, they are not without advantages. The first benefit is increased control of the location of the applied field on the plasma. Another observed advantage is that, when pulsing, the stroke length is short enough to prevent adverse interactions between the plasma and the free electrons. The third and perhaps the greatest advantage of unsteady propulsion systems is that they can operate without an electrode. In steady propulsion systems electrode erosion is often the most significant life-limiting factor to be considered. The unsteady thruster, by eliminating this component, can have a substantially longer mission life.

1.1.3 Electrical Background

The PIT is unique in that it generates thrust through induction. Induction can be viewed as magnetic field entrainment; a changing current through a coil drags a magnetic field through its aperture. A simple way to think of this is as a sort of electrical momentum, in that no force can be generated by a constant current. The change in current, usually written as dI/dt, is the key factor in the operation of the

PIT. This concept can is seen in eq.(1.4):

$$v_L = L * \frac{dI}{dt} \tag{1.4}$$

From this equation it is clear that the induced voltage drop, shown above as v_L, increases as the dI/dt increases.(15) This voltage can also be seen as an electromagnetic force (emf) that is generated. This relationship is derived from Faraday's law which relates induced coil voltage (e_L), cylindrical coil geometry (N # of turns), and the rate of change of flux through the window of the coil ($d\phi/dt$):

$$e_L = -N * \frac{d\phi}{dt} \tag{1.5}$$

These equations were developed by analyzing the magnetic fields around copper coils, but the concepts can be applied to a plasma using the generalized Ohm's Law, an equation used to understand the relationship between momentum, current, and the magnetic and electric fields.(30)

$$0 = \sigma * (\vec{E} + \frac{\vec{V}}{c} \times \vec{B}) - \frac{\sigma}{e * n_e} * (\frac{\vec{j} \times \vec{B}}{c} - \nabla p_e) - \vec{j} \tag{1.6}$$

$\vec{V}$ is the hydrodynamic velocity; $\vec{E}$ is the electric field; $\vec{B}$ is the magnetic field; σ is the electrical conductivity; e is the electron charge; n_e is the electron density; $\vec{j}$ is the electrical current; ∇p is the plasma pressure gradient, and c is the speed of light. Most plasma interactions can be derived from this general equation.

A large dI/dt can be generated in a number of ways, but the easiest method is to store a large amount of energy in a capacitor and discharge the energy through an induction coil. This simple circuit is the design basis for the PIT.

While this circuit is quite basic and easy to analyze, the actual operation of the PIT is much more complicated, a fact that has been noted by researchers since the inception of the idea and will be addressed in greater detail in the computer modeling chapter.

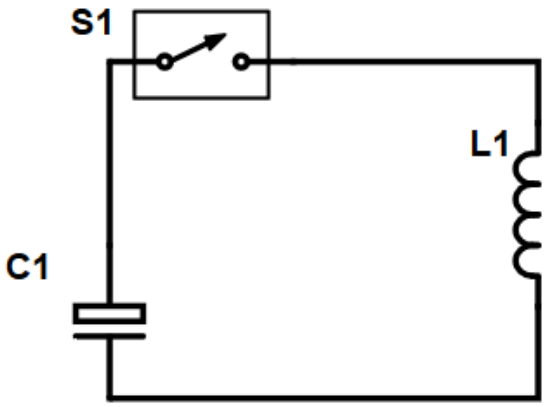

Figure 1.1: Simple PIT Circuit Diagram

1.2 Statement of Problem

Electric Propulsion is quickly moving to the forefront of research as the main mode of space travel. Most of this research is being done on Hall thrusters, gridded ion thrusters, and electrospray thrusters as they currently have the highest efficiencies. The two main problems that these thrusters have is that they cannot scale up to the MW range and that they utilize electrodes that suffer from severe erosion. This is where the PIT has demonstrable advantages.

Most research on the PIT has utilized spark gap switches which also erode fairly quickly. To resolve this issue, modern designs have started implementing solid state switches. The problem is that these switches, thus far, have not been able to handle the large power surges required for the PIT acceleration mechanism. In an effort to alleviate this issue, PIT designs were scaled down to fit the tolerances of the solid state switches. The efficiency of the PIT scales with it's geometry so these new designs were less efficient than the original, larger designs. This loss in efficiency is primarily due to the amount of propellant that does not fully couple with the accelerator coil.

Two courses of action represent possible solutions to this problem. The first option

is to find and implement better switches that can handle the power requirements of the larger designs without becoming the life-limiting component of the thruster. The second option is to find a way to promote more complete plasma coupling over the acceleration coil. These two solutions are more thoroughly investigated in the chapters titled "Trade Study" and "Improvements to Plasma Coupling."

1.3 Computer Model

Introduced in this thesis is a new method of simulating PITs. This starts with three inputs: a propellant, a coil geometry, and a guess value for the decoupling length (z_0). The code uses the molar mass and ionization potential of the propellant to calculate the Alfvén velocity.(2) This, in turn, is used to calculate the critical mass (m_c) and energy (e_c) for the given thruster geometry. This then feeds into a model similar to that used by Dailey & Lovberg in 1979 in their work on the 1-meter coil. After one iteration, the energy of the system is totaled and checked against the initial energy stored in the coil ($E0$). If the total energy of the system exceeds the initial energy, the initial guess for decoupling length was too short and a second iteration with a new z_0 value. This process is repeated until the energy is balanced. This will result in the decoupling length required for the given thruster.

Chapter 2

LITERATURE REVIEW

This review is broken into two major sections. First it addresses the history and development of the Pulsed Inductive Thruster (PIT). This section is separated into three subsections, identified by K.A. Polzin: early research, full-system development, and state-of-the-art technologies.(26) The second section identifies the problems of unsteady firing in electric propulsion systems and the significant attempts that have been made to overcome them.

2.1 History of the Pulsed Inductive Thruster

Research Phase (1965-1973)

The first PIT designs appeared in the mid-60's with C. L. Dailey and R. H. Lovberg. Dailey was investigating the plasma acceleration mechanism at TRW Space Systems(5) while Lovberg was analyzing the current sheet micro-structure at the University of California at San Diego(18). During their work together several years later, they were able to achieve both of their goals and determine the plasma momentum in three dimensions as well as the individual contributions of each accelerating mechanism on the overall momentum of the plasma.(11) Dailey & Lovberg had originally set out to investigate the results of experiments done by themselves and others several years earlier, showing that large ion currents were present in inductive-impulsive accelerators. They began their investigation by determining whether the plasma acceleration was purely in the axial direction (z) or if there were components in the radial (r) or azimuthal (θ) directions. If any θ-acceleration should be observed, this would indicate

that the accelerated plasma was rotating. A rotating plasma field would suggest sev-

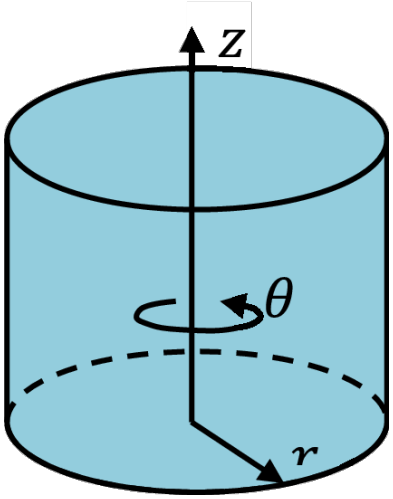

Figure 2.1: Cylindrical Coordinate System

eral things about the acceleration mechanism. First, energy must go into the plasma to cause rotation. This energy is considered lost as it does not contribute to the z-acceleration without some recapturing mechanism downstream. By following the generalized Ohm's law, it can be seen that a rotating plasma field would be due to a substantial contribution of ion current in the overall induced current sheet. The presence of a strong ion current would introduce additional complexity to the system by adding a component to the acceleration mechanism through the Lorentz body force.

The curious thing about these early experiments was that there was a distinct lack of an electrostatic space-charge field. This field must be present in a current sheet that is primarily due to electron flow (an assumed feature of an inductive accelerator). This lack implied that there must be an ion current of magnitude nearly equal to that of the electron current. This finding made sense and was useful in describing the operation of accelerators utilizing electrodes, but also seemed to fit with inductive accelerators. This seemed strange for certain types of inductive thrusters as it would require a greater axial torque than should be possible given the geometry of the

device, specifically that of a planar coil accelerator.

Going forward with this information, tests were performed comparing the two accelerator types, specifically the θ-pinch and the parallel plate accelerator. Using a Schlieren technique to visualize the plasma, no rotation was observed. However, in the θ-pinch, a strong radial electric field was present, and in the parallel plate device there was only a very weak axial field.

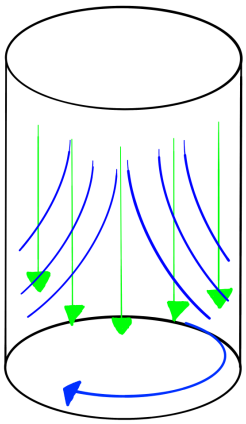

Figure 2.2: θ-Pinch

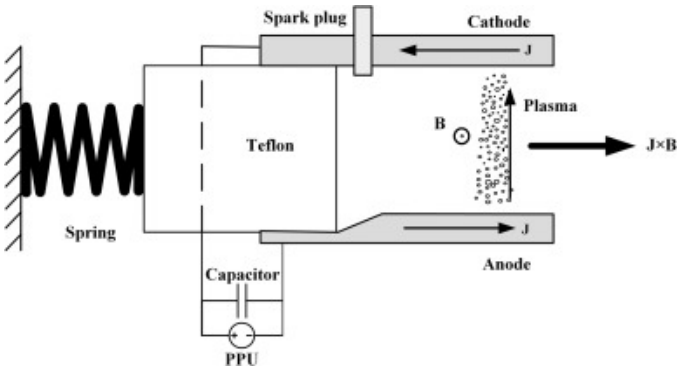

Figure 2.3: Parallel Plate

Counter to what was implied by the earlier experiments, this discovery seemed to show that substantial ion currents could only be found in electrode-based devices. The logical next step was to perform similar tests on the planar spiral geometry used

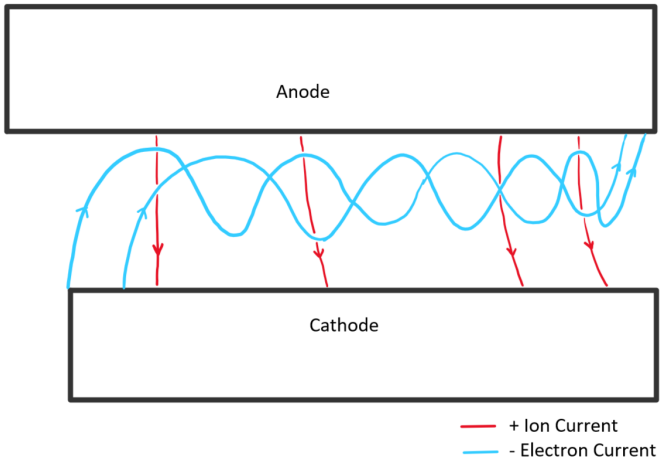

Figure 2.4: Ion Current Path

in a PIT. In an idealized and preionized case, Spitzer showed mathematically that a strong ion current, equal to the electron current, would be observed.(28) The problem with this proof are the assumptions necessary to ensure its validity. In his model, Spitzer assumed a constant E and B field. In actuality, by generating an ion current, the E field would have to fluctuate. Connected with this, in an inductive thruster, the B field is entirely induced from the electric current and thus can only remain constant as the change in current remains constant, which is not the nature of an unsteady accelerator.(13)

By employing a combination of miniature coils and laser scattering techniques, Dailey and Lovberg found that there was no detectable θ-acceleration and thus the ion current was negligible, demonstrating that the acceleration was entirely the product of the axial electric field. Two major factors contributed to this electric field. The principal factor was the polarization field due to the induced plasma electron current. The second factor was the added pull of the negative electron pressure gradient on the leading edge of the plasma sheet.

This work was done concurrently while developing a prototype accelerator.(11)

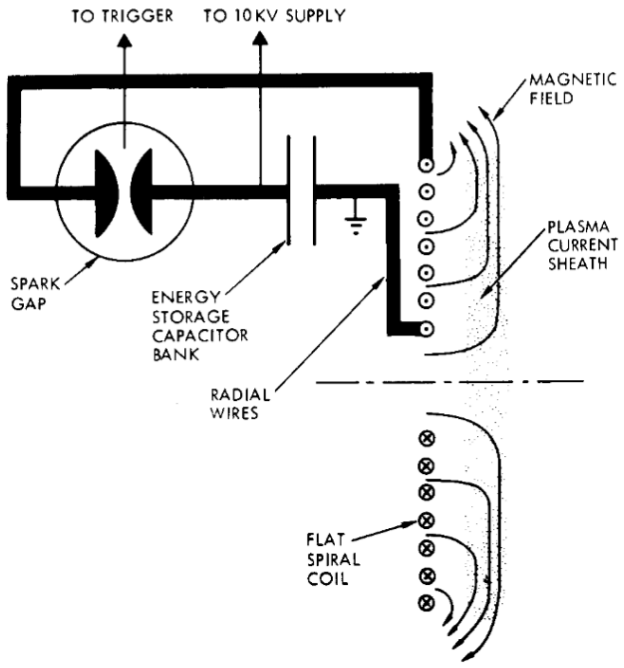

Figure 2.5: 20cm Accelerator Design

The first set up used a 20 cm diameter planar coil inductor. Using this set up, Dailey and Lovberg were able to achieve a thrust efficiency of 5.5% at a corresponding specific impulse (Isp) of about 1200 seconds. Dailey and Lovberg went on to duplicate much of this work using a 30 cm diameter coil.(7) The Isp and thrust efficiencies were significantly improved using this larger geometry, yielding values of 1470 seconds and 18% respectively. This was the first major scaling factor encountered in relation to PIT development and will be discussed in greater detail below.

These two prototypes were tested against two variable conditions: propellant distribution and preionization. The two methods of propellant distribution were to run the accelerator in an ambient/static fill scenario and a pulsed-injection scenario. The static fill method involved filling the entire test chamber uniformly with the propellant gas. The pulsed injection method was meant to simulate the actual operation of a thruster in space, with a pulsed gas injector spreading the propellant gas over the

surface of the thruster. As might be expected, the static fill method yielded a much greater Isp and efficiency in both thruster geometries. In the static fill test, the total force delivered was greater, and it reached its maximum thrust in a shorter period. Initially, this could be attributed to the greater total mass available for acceleration in the static fill test; however, another, less intuitive phenomenon was observed: the pulsed-injection test did not yield the expected "snowplow" of the non-ionized propellant. Instead, the accelerated plasma passed through the downstream propellant gas. Because of this, less mass was being accelerated and consequently the mass that was being accelerated, did so in a much shorter period. In doing so, the plasma current sheet decoupled before the coil current could reach its peak, yielding a smaller total impulse.

Another interesting note about the pulsed-injection method was that, while the magnitude of the force remained roughly constant, the change in thrust in relation to time could be influenced by the location of the concentration of propellant in relation to the face of the thruster. When the gas density was greatest towards the outer radius of the coil, the force took much longer to reach its peak.

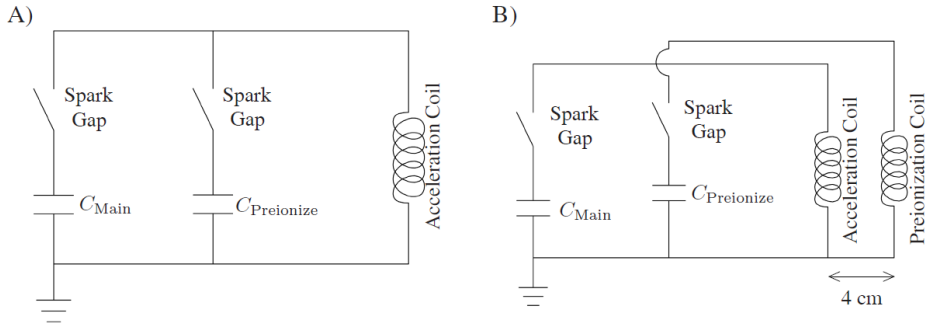

Figure 2.6: Preionization Circuits

When testing the effects of propellant preionization, three options were available: no preionization, preionization through "geometry A", and preionization through

20 cm Diameter				
Fill Type	Static Fill		Pulsed Injection	
Preionization	No	Yes	No	Yes
η	6.2%	11%	5.5%	-
Isp	1350s	2800s	1200s	-
C	$1.75\mu F$	$3.9\mu F$	$3.9\mu F$	-

Table 2.1: 20 cm Diameter Performance Data

30 cm Diameter				
Fill Type	Static Fill		Pulsed Injection	
Preionization	No	Yes	No	Yes
η	17%	-	5.0%	18%
Isp	1430s	-	500s	1470s
C	$6\mu F$	-	$6\mu F$	$6\mu F$

Table 2.2: 30 cm Diameter Performance Data

"geometry B." Theoretically, by preionizing the gas, all of the energy of the main pulse would go into generating the current sheet, thus increasing the available energy to the acceleration mechanism. While both geometries achieved the goal of ionizing the propellant, only geometry B proved to be advantageous to the thruster overall. Using geometry A, the process of ionizing the gas accelerated it away from the coil, reducing the available time and energy that could be coupled into the current sheet by the main pulse. Using geometry B, the propellant accelerated toward, and compressed against, the face of the main coil, consequently increasing its density and conductivity.

Not every combination was tested on each thruster, but the results of the tests completed are shown in the tables below. The preionized values shown correspond to geometry B.

	30cm	1m
N	2	1
Coil #	-	36
C_B	$6\mu F$	$20\mu F$
V	14.8kV	20kV

Table 2.3: 30 cm vs 1 m accelerators

Thruster Design Phase (1973-1988)

Up until this point, most work in the field of unsteady plasma acceleration had been rather academic, more concerned with understanding the phenomenon than using it practically. With the 30 cm diameter thruster built in 1973, the work shifted from theoretical research to an increased focus on full thruster development.(7) Most of this development was done at TRW over a period of a decade and a half.

The starting point for this continued development was to pursue the performance discrepancy noted between the 20 cm accelerator and its scaled up 30 cm counterpart. The next logical step was to develop and test an even larger diameter accelerator. Consequently, the first 1-meter diameter thruster was completed in 1979.(6) The size of the coil wasn't the only change. As seen in Table 2.3, there were many other changes to try to improve efficiency and tailor key performance parameters. The main thinking behind the geometry scaling was that by increasing the diameter, the inductance of the coil would increase and consequently, the decoupling length would be larger.

Initial tests of this thruster were promising. Thrust efficiencies and *Isp* were calculated at 42% and 1540 seconds respectively. These results were obtained by taking field measurements and integrating the Lorentz body force. Repeating these tests with a thrust balance gave values for an *Isp* and a thrust efficiency of 1236

seconds and 25.4% respectively.(6) The integral seemed to overestimate both. While these values were not as high as had been originally predicted, they were still a major improvement to previous designs and proved the theory relating the scale of the geometry and the performance of the thruster.

This success provided a starting point for the next wave of designs, though they were all based on and quite similar to the 1-meter diameter thruster discussed above. The next two major designs created by Dailey & Lovberg at TRW were the PIT MkI and MkIV.(8)(9) The MkI was a duplicate of the 1-meter thruster with a few minor geometric changes. The MkIV was scaled down to two-thirds the size of the MkI thruster and could operate in one of two different modes: ringing or clamped. In the ringing mode, the charge was free to build up on either side of the capacitor allowing it to "bounce" back and forth, giving the charge and current an oscillatory motion with respect to time. In the clamped mode, diodes were used to force the current to flow in one direction. This was intended to prevent the "backswing" of the current from undoing the majority of the work initially done by the acceleration mechanism.

An interesting feature of the MkI is that it had only 24 coils as opposed to the 36 used by its predecessor. Even with fewer coils, the MkI still showed roughly the same performance as the 1-meter thruster. As was expected with scaling down the size, the MkIV did not perform as well as the MkI.

The decrease in performance of the MkIV was greater than could be explained by the reduction in scale. When the phenomenon was investigated further, it was found that not all of the plasma was being accelerated away before the second half of the firing cycle. During the second half of the cycle, the coil would stay coupled to some of the plasma, effectively pulling it back, greatly reducing the performance of the thruster.

Contemporary Research (1988-Present)

The next design was the PIT MkV, the most well-known and analyzed thruster of its type; its design and analysis were published in 1993.(10) Most modern designs are still based on this model. As with previous designs, one major objective of the MkV was to maximize the dI/dt. The MkV was also designed with more precise tolerances so as to minimize the parasitic inductance of the circuit and consequently improve the inductance ratio.

The biggest improvement made in the MkV was the implementation of Marx generators, which convert a low DC voltage into a high voltage pulse.(21) A classic Marx generator works by charging a number of capacitors in parallel and then discharging them in series.

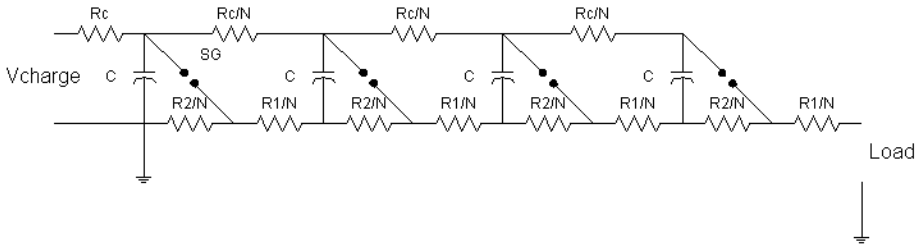

Figure 2.7: Marx Generator

The MkV used two $4.5\mu F$ capacitors on each coil, thus doubling the voltage available for each shot. Each capacitor was charged to 15kV, so the total available voltage drop across the coil was 30kV, resulting in roughly 2kJ of available energy per pulse. Nine of these coils were arranged at 20 degree intervals around a circle, equidistant from each other as to maintain a uniform magnetic field over the face of the coil. This also served to minimize the parasitic inductance. The MkV was able to operate with a total inductance of 740 nH, of which only 60nH could be attributed to parasitic inductance.

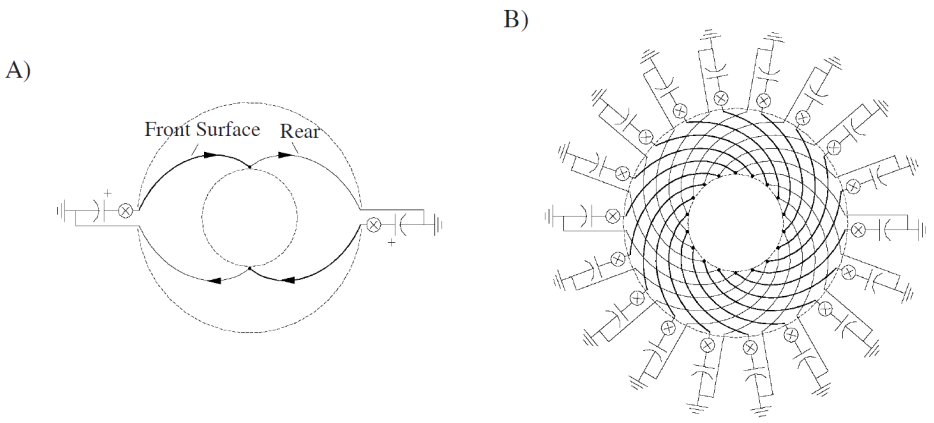

Figure 2.8: Marx Generator Arrangement in the MkV

To maintain these values and keep the magnetic field uniform as designed, all nine circuits (18 spark gap switches) had to be triggered within a very tight time period, t, relative to each other. For this specific circuit, that window was limited to 5 nanoseconds. If one of the parallel gaps fired more than t before its counterpart, the corresponding drop in voltage for the second gap would be too great and it would not fire at all. To overcome this a master pulse generator had to be used. In addition, each lead connecting the pulse generator to the switches had to be of equal length, and they had to be long enough to keep the grounding plate beyond the decoupling length of the coil. Otherwise, the plasma would only accelerate up to a distance that equaled the distance between the grounding plate and the coil. A safe length for this design was determined to be 40 cm. Another aspect of this system that had to be carefully monitored and controlled was the pressure within the spark gaps. This pressure had to be adjusted to ensure they all fired at precisely the same moment relative to when they received the signal from the pulse generator.

As shown in Fig. 2.9 and Fig. 2.10, the gas injection system uses an annular cone as a nozzle to direct the propellant gas down towards the face of the coil. This was the same system that had been used since the MkI. The pulsing mechanism was very

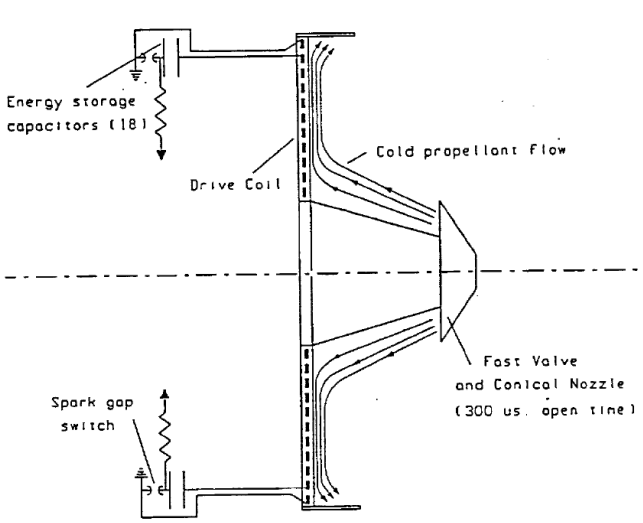

Figure 2.9: Propellant Injection System

similar in design to that of a loudspeaker, in that it was driven by a permanent magnet and a coil. The insulated coil housing was secured to a stainless steel diaphragm. When a 5-joule pulse was sent through the coil, the diaphragm would move down 0.5 mm, creating a circular opening to allow gas to escape from the propellant chamber. This internal mechanism can be seen more clearly in the figure below. The gas would then pass through the above-mentioned nozzle which would direct it in such a way to spread it as evenly as possibly across the face of the coil. A ring of glass plating was placed around the outside edge of the coil to prevent the gas from spilling out and to help smooth the gas distribution.

For propellant there were two principal options: ammonia and hydrazine. The advantage of hydrazine was its already heavy implementation in existing space operations, and the devices for its storage and handling were already well-established. The main drawback of hydrazine was the amount of heat it released upon ionization. In a vacuum, most of this heat would be absorbed by the thruster and contribute to the existing cooling problem encountered by all extra-atmospheric energy systems.

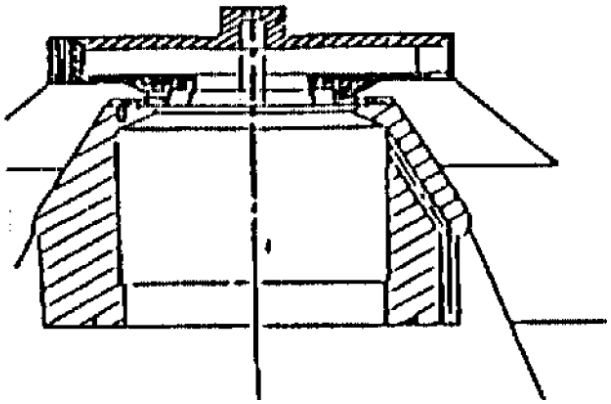

Figure 2.10: Propellant Injection Valve

Ammonia was also a good choice as it is easy to handle and was readily available. In the end it was decided to run tests using each of these propellants. In the case of ammonia, a nitrogen-ammonia mixture was used in place of ammonia as a pure substance.

The ammonia tests were performed using a range of voltages from 12-16kV. Testing along this range revealed something interesting about behavior of PITs. When analyzing the data collected from these tests, it was noted that, as less mass was loaded into the accelerator, the *Isp* would increase. This would be expected as more energy could be deposited into less mass, resulting in higher exit velocities and consequently higher *Isp*. What wasn't expected, however, was the observed maximum value of thrust efficiency. There seemed to be a minimal limit on the mass bit used. Loading the accelerator with less mass than this limit would decrease the thruster's efficiency. This has been noted as the critical mass. This has to do with the thruster's ability to move the mass past the decoupling length at the proper time. If the mass bit is too large, the plasma will not be able to decouple before the current starts to reverse direction, resulting in a lower Isp and thrust efficiency. If the mass bit is too small, the plasma will decouple too early and will not be able to capture all the

energy available to it through the coil. This results in an higher in *Isp*, but a lower thrust efficiency. It is through this relationship that an optimal value of both thrust efficiency and Isp can be found at the critical mass.

In the case of the hydrazine, no critical mass could be determined as the models could not be matched to any of the test data. Another note on the hydrazine is that when tested at similar voltages to ammonia, the hydrazine would produce markedly lower plasma temperatures, resulting in poor ionization of the propellant gas and a lower efficiency. With these findings, no further hydrazine tests were conducted.

Using the data gathered in the course of this work, Dailey & Lovberg estimated that, using the technology of the time, they could construct a 1.2 MW engine with a specific mass of 0.25 kg/kW. Owing to PITs efficiency scaling to its size, this engine would far surpass any other thruster of its class.(10)

2.2 Unsteady Firing Issues

As stated in the introduction, the concept of an unsteady propulsion system is not without drawbacks. The main problem encountered in the development of the PIT was the erosion of the spark gap switches used to pulse the coils. The most notable attempt to abate this issue is the work currently going on at NASA's Marshall Space Flight Center (MSFC).(1)

One of the major goals of this project was to replace the spark gap switches with thyristors. In Fig.2.11, the thyristor implementation is shown next to an additional diode, put into place to prevent the circuit from ringing. Thyristors currently available have significantly lower voltage and current tolerances than spark gaps, thus the design of this PIT had to be scaled down accordingly.(24) This scale is shown in Fig.2.12 with the inner diameter of the coil at 100mm and the outer diameter at 270mm. This scale is just over one-fourth of the size of the MkV. As mentioned

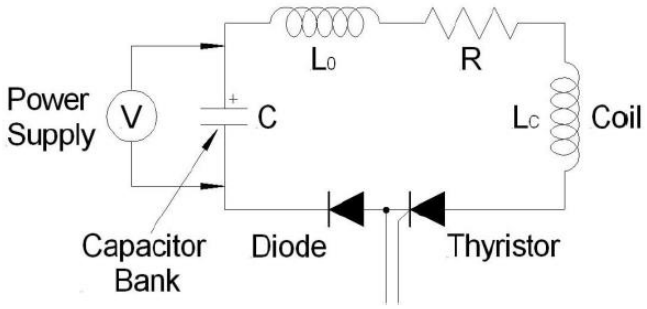

Figure 2.11: Small PIT Circuit

previously with the work done in 1979, the size of the coil is proportional to the efficiency of the thruster.(6)

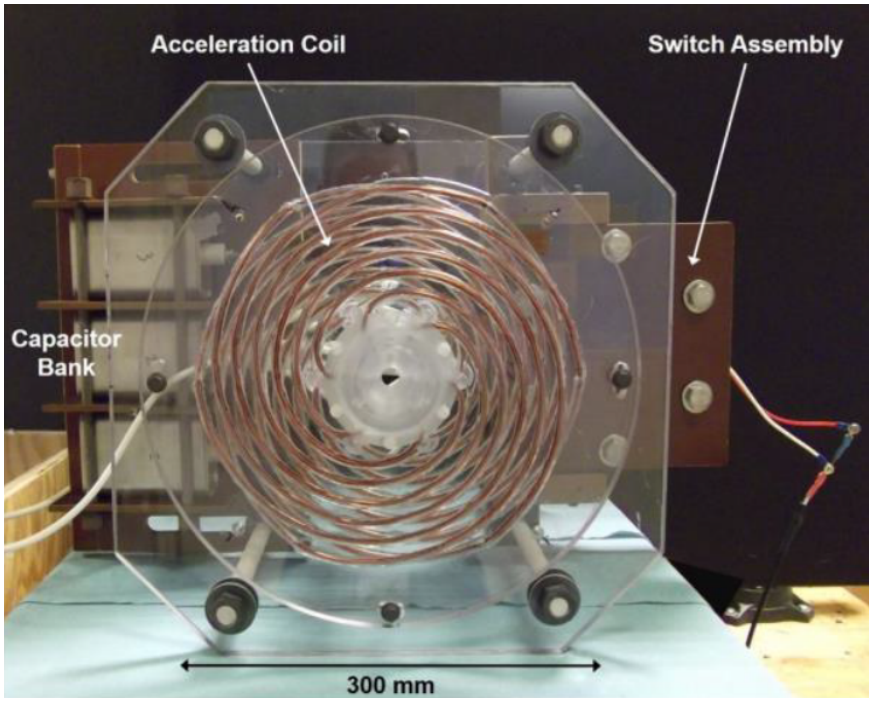

Figure 2.12: Scaled Down Thruster

Though the decrease in performance was noted, the actual efficiency of the small PIT was never published. The reason for this omission was that the efficiency was not the focus of the study. The study was to test the capability of thyrsitors as triggers when implemented into the firing circuit.

Before real testing could be done on the firing circuit, certain parameters such as decoupling length and circuit inductance had to be determined. A PIT cannot run without a plasma to couple with, so rather than do the preliminary testing in a vacuum chamber, a "dummy plasma" in the form of a copper plate was used. This copper plate would also be more convenient in measuring results and give more consistent values. Most of the testing rig was mounted using wood and plastic in an attempt to minimize interference. The results of this test can be seen in Fig.2.13 showing the measured total inductance and the calculated coil inductance. These values are plotted against the distance of the copper plate from the acceleration coil.

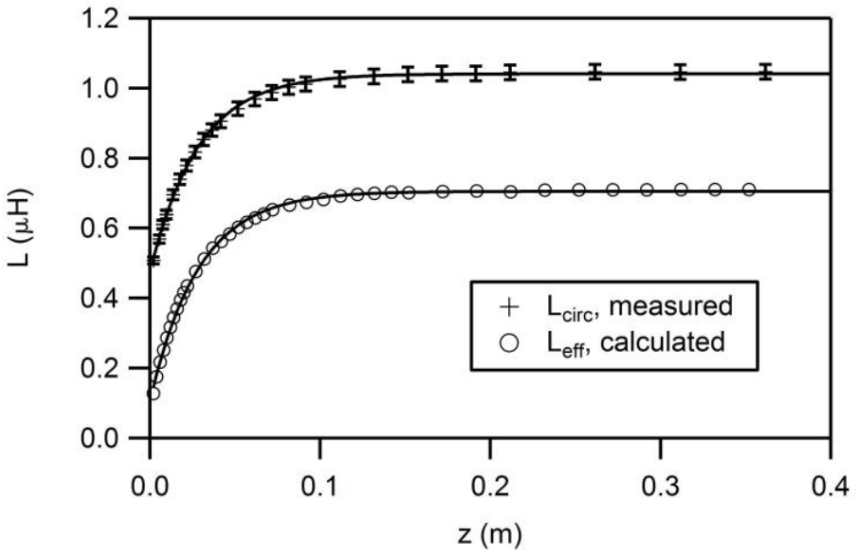

Figure 2.13: Measured and Calculated Inductance of the Small PIT

The curves shown in Fig.2.13 represent Eq.(2.1) which was used as a best fit curve for the measured data points.(20) Curve fitting was one of the methods used in determine some of the desired parameters such as stroke-length. These fitting parameters are shown in Table 2.4. These tests were all done at a relatively low voltage of 1100V.

-	Quantity fit to:	
Fitting Parameter:	L_{eff}	L_{circ}
L [nH]	705 ± 3	1041 ± 7
z_0 [mm]	57 ± 1	57 ± 3
k_0	0.92 ± 0.01	N/A
ξ^2/ν	0.4	0.1

Table 2.4: Fitting Parameters of the Small PIT

$$L(z) = L_\infty * (1 - k_0^2 e^{-2\frac{z}{z_0}}) \tag{2.1}$$

After determining the basic operating characteristics of the thruster, the circuit was tested at higher voltages ranging up to about 3000V. At the highest voltage tested, the current reached a peak of 7.4kA. As shown in Fig.2.11, the design includes a diode which forces the PIT into a clamped mode of operation. These tests were run through the failure of the diode.(31) Fig.2.14.a shows the waveforms before the failure of the diode and Fig.2.14.b shows the waveforms after the failure of the diode. After the diode fails, the circuit switches into a ringing mode of operation.

An interesting characteristic about the thyristor can be seen quite clearly in these figures. Even though the switches were triggered at $t = 0$, nothing happens until about $t = 10\mu s$. The delay time in the thyristors was found to be $9.6\mu s$ before diode failure and $7.3\mu s$ after diode failure. In the ringing case, this delay decreased as the voltage applied across the switch was increased. Only the four shots were measured, so no reliable trend was developed.

Vacuum tests were also conducted in addition to these bench-top tests. The thyristors were tested at rates up to 20Hz without any signs operational detriment. The test of the PIT as a whole, however, was limited to 2Hz due to the feed-gas

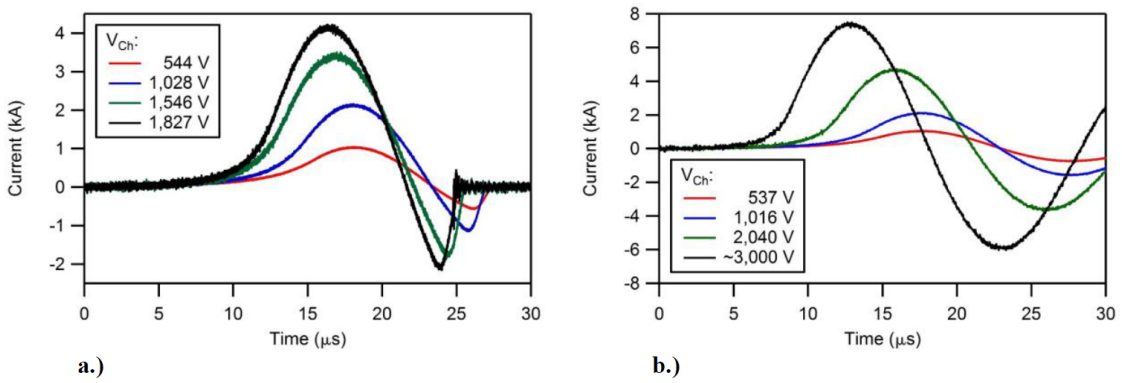

Figure 2.14: Current Waveforms in Small PIT Testing

pulsing system. In most tests, a plasma would start to form behind the coil after about 15 pulses. This plasma created an easier path for the current to follow, causing the insulation to melt and the circuit to short.

At the conclusion of this work, the thyristor-diode combination proved to work well up to 2kV and 20Hz. Putting multiple diodes in parallel was recommended to decrease the likelihood of diode failure, but these builds would increase the total circuit resistance. Another suggestion for future work was the implementation of gate turn-off thyristors (GTO) or insulated gate bipolar transistors (IGBT) as these would also block any reverse current.

Chapter 3

TRADE STUDY

This chapter focuses on several of the types of switches available for use in a PIT. These switches fall into two categories. The first category is identified as conventional relays. These are older switching mechanisms that must employ moving parts or gaseous mediums. The second category covers solid state relays.

3.1 Conventional Relays

3.1.1 Spark Gap

Spark gaps are currently the main form of switch used in PIT's. They are cheap, well understood, and can operate in a wide range of environments.

Design and Operation

A spark gap is a switch that employs two electrodes separated by gaseous medium. A large voltage difference is built up across the two electrodes. When this voltage exceeds the breakdown voltage, the gas between the electrodes ionizes, allowing current to flow from one electrode, through the gaseous medium, to the opposite electrode. A benefit of spark gaps is that, in theory, there is no limit to the voltage or current they can carry. By varying the distance between the two electrode and adjusting the gas pressure within the switch, spark gaps can be calibrated to fire in almost any scenario.

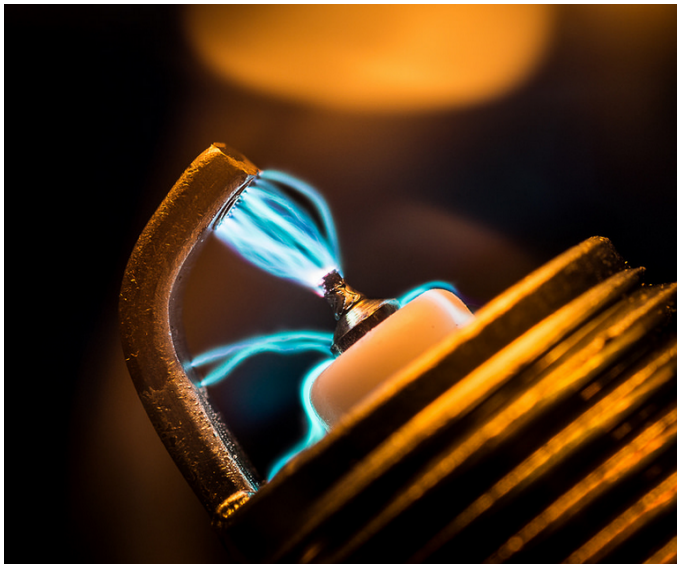

Figure 3.1: Spark Gap

Electrode Erosion

The biggest drawback to spark gap switches is their relatively short life. At the onset of the spark a high-speed jet of super-heated, ionized vapor is produced near the surface of the first electrode. This can boil the surface of the electrode, and thus, some of the ionized stream will be comprised of the material of the electrode itself. These jets can reach speeds of 10^4 m/s and temperatures of 40,000 K, hitting the opposite electrode with such force and heat that they leave small, but measurable craters.(27)

3.1.2 Mechanical Relays

Operation

One idea to combat this issue is to eliminate these destructive jets by eliminating the gaseous medium. A device that can operate in exactly this manner is the electro-mechanical relay. This device operates in the same manner as the average light switch.

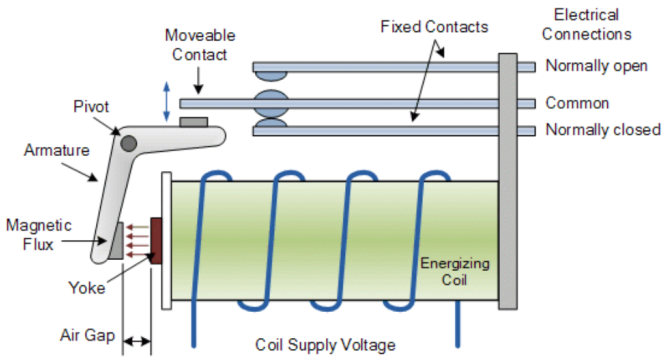

Figure 3.2: Electro-Mechanical Relay

A light switch is operated by manually manipulating a contact to complete a circuit, like someone moving a lever. An electro-mechanical relay operates in exactly the same way, except instead of a hand moving the contact, it is done by an electromagnet as shown in Fig. 3.2. These contacts can be moved into position in total vacuum, thus eliminating the gaseous medium.

Vacuum Arcing

This, however, does not entirely eliminate the problem of erosion. Contrary to what is commonly believed, an arc can occur between two electrodes without any kind of medium between them. This does not manifest as a visible spark as is commonly seen when using a gaseous medium; rather, it is observed as a glow of one of the electrodes. Without a medium, the gap is bridged by charged particles boiled off one of the electrodes. The observed glow is caused by the impact of these charged particles on the electrode.

As the gap between the electrodes decreases, there is a point where the charge jumps the remaining distance, eroding the electrodes before they can be brought into full contact. Consequently, the mechanical relay does not entirely eliminate electrode erosion, but it does stand as an improvement over the spark gap in this regard.

Alternative Hardware

As mentioned, spark gaps require an entire subsystem to maintain the proper gas pressure within the switch. Mechanical relays only require a small electromagnet to control triggering. This reduction in mass significantly improves the specific mass of the spacecraft.

There are a couple major weaknesses of electro-mechanical relays. The biggest of these drawbacks is that they have moving parts. Any moving part has a life limited by the number of cycles the material can withstand before failure. This particular style of em relay has a life of about 300,000 cycles. At 20Hz, this gives a total operation life of a little over 4 hours. Mechanical relays are also incredibly slow, switching at speeds measured in milliseconds. One of the biggest problem with using one of these relays on a PIT is that these switches operate using magnetism. The act of firing could cause erratic behavior or even failure in these switches if they are not properly protected.(32)

3.1.3 Thyratrons

History and Operation

Work on thyratrons started in the 1920's.(23) The design was meant to be an improvement on existing vacuum tubes by combining them with gas rectifiers. The basic design of a thyratron consists of an anode, a cathode, and a control grid. A voltage is placed across the anode and cathode, but while in the off-state, nothing can happen. The control grid prevents the cathode from "seeing" the anode as the grid is at a slightly negative charge relative to the cathode. The thyratron is put into the on-state when the control grid is brought to a more neutral state. The grid is no longer repelling electrons from the cathode, allowing ionization of the gas to

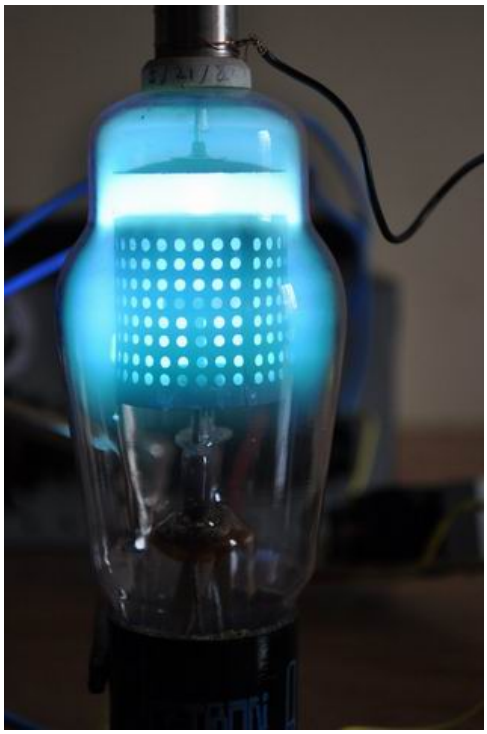

Figure 3.3: Thyratron

occur and a current to form between the anode and the cathode. Once this current is established, the thyratron cannot be switched into the off-state until the current is no longer great enough to reach between the anode and the cathode.

Reduced Electrode Erosion

Unlike spark gaps, the electrodes in hydrogen thyratrons don't erode nearly as much as the discharge is spread through much of the plasma rather than in one concentrated arc.

Heat Dissipation

In space, the only available mode of heat transfer is radiation. Radiation on its own is not an effective way to remove heat from an object. Because of this, the thyratron has a major issue to overcome before it could be implemented in any space systems.

Thyratrons must reach a high temperature before they can act as switches; this temperature is usually achieved through filament preheating. In most of its previous uses, the thyratron was within the atmosphere and could have most of its excess heat convected away. On a PIT operating in space, this is not an option. The excess heat would likely build up within the device and melt the internal components.

3.2 Solid State Relays

3.2.1 Thyristors

The term "thyristor" is a combination of "transistor" and "thyratron" because it operates in the same manner as a thyratron, but instead of using a gaseous medium, it employs the use semiconductors as in transistors.

Operating Principles

While spark gaps are relatively straightforward, the workings of thyristors are a little less transparent. A thyristor is a solid-state switch that operates through the use of n-type and p-type semiconductors.(22)

N-type semiconductors utilize material that has an excess of electrons that are free to move about in the material. When a voltage is applied, un-bonded electrons move relatively freely and a current can flow.

In contrast, p-type semiconductors have an excess of holes (lack of electrons). In this material, electrons jump from hole to hole, creating a similar free movement of electrons as in the n-type.

Placing p-type and n-type semiconductors in series creates a diode. As a result, current can only pass through them in one direction. Adding another semiconductor to this arrangement creates a bipolar junction transistor (BJT)–an electronic switch.

Transistors can be built with a p-n-p or n-p-n arrangement. The first semiconductor in the sequence is the emitter, the thin middle is the base, and the third is the collector. A large voltage can be placed across the emitter and the collector, but no current will flow. By having three layers of alternating semiconductors, there will always be a diode blocking the current, regardless of the direction of flow. The voltage will create a forward bias (conducive to flow) in one of the junctions, and a reverse bias (preventing flow) in the other. To permit electrons to flow from the emitter to the collector, a small control charge must be placed across the reverse biased junction using the base section. This will cause the second junction to become forward biased and will allow current to flow freely from the emitter to the collector. As a result, transistors can be used to boost small signals sent through the base.

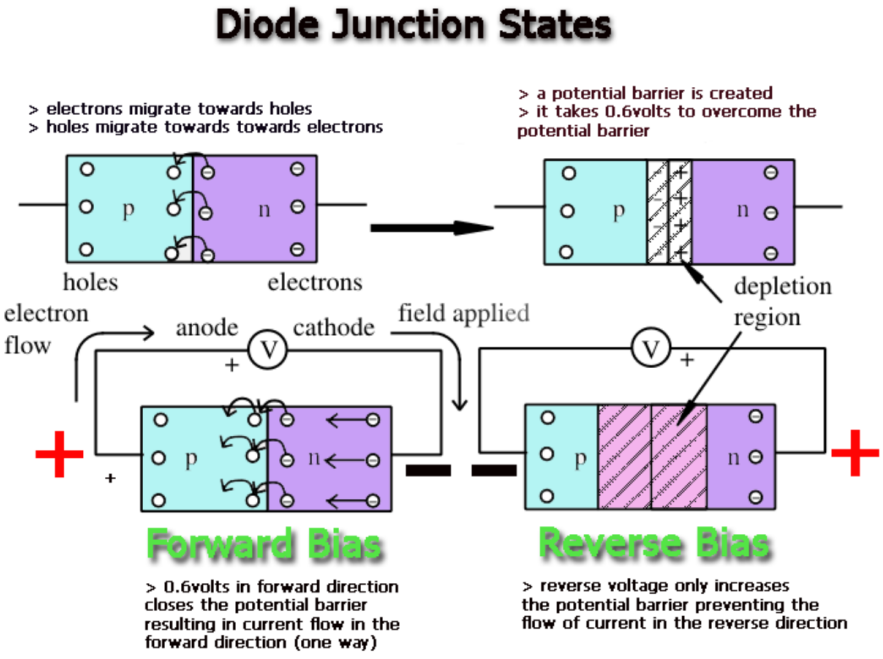

Figure 3.4: Junction States

3.2.2 Silicon Controlled Rectifiers

The most basic thyristor is a Silicon Controlled Rectifier (SCR). Th SCR works by configuring a p-n-p transistor and a n-p-n transistor as shown in Fig.3.5. By

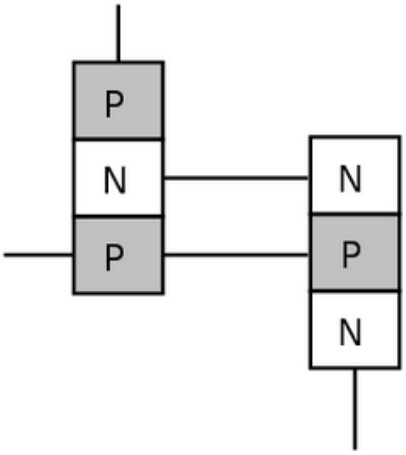

Figure 3.5: Simple Thyristor

connecting the emitter of one transistor to the base of the other, the transistors no longer act as amplifiers, but work together to make one switch with two distinct states: on and off. While thyristors can handle greater loads than individual transistors, their robust nature requires a greater power draw, meaning greater power losses within the device. In order to initiate the on-state, all of the semiconductor layers must be brought to a forward bias, or a state in which they can interact with their neighboring layers. Having only the two states, thyristors make ideal switches. However, once in the on-state, the thyristor will remain on regardless of the gate current. A thyristor can only be turned off by the cessation of current.

3.2.3 Metal Oxide Semiconductor Field Effect Transistors

Metal oxide semiconductor field effect transistors (MOSFETs) are different from BJTs in that instead of directly influencing the bias of an entire semiconducting

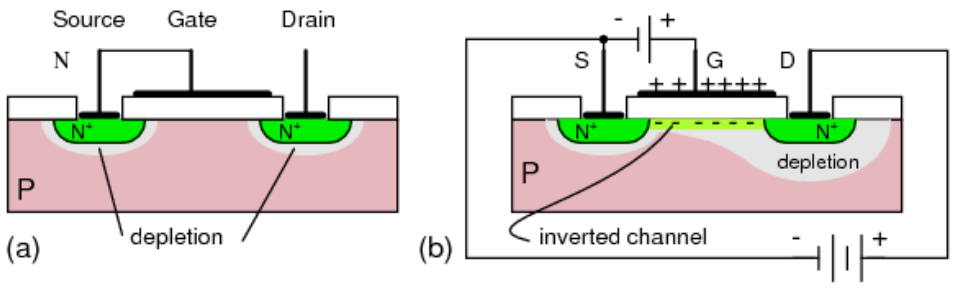

Figure 3.6: MOSFET

layer, a thin path is created along which current can flow.(14) As shown in Fig.3.6 MOSFETs consist of p-type substrate, two n-type contact layers, a source, a body, a drain, and a gate. The MOSFET in its off state has no way for current to flow as the source, drain, and gate are all completely separated.

In BJTs the gate is in direct contact with the interim material, in this case that material would be the p-type substrate. In a MOSFET the gate is separated from the substrate by a thin layer of insulating material. As seen in Fig.3.6b, when a positive charge is applied to the gate, it attracts a negative charge in the substrate, creating a path of electrons between the two n-type layers along which current can flow. This operates in the same way as the two plates in a capacitor.

This method serves to be a great benefit. As only a small path is created instead of an entire semiconducting layer, the current required to create this bridge is much smaller than that required by a BJT. For this same reason, MOSFETs have the highest switching speed of all relays considered in this study.

3.2.4 Insulated Gate Bipolar Transistors

As mentioned above, the SCR is made by combining two BJTs to create a relay that consists of four layers. In this same spirit, the Insulated Gate Bipolar Transistor (IGBT) is made by combining a BJT and a MOSFET as shown in Fig.3.7. The

MOSFET and BJT share an emitter, but the collector of the MOSFET is attached to the gate of the BJT.(3)

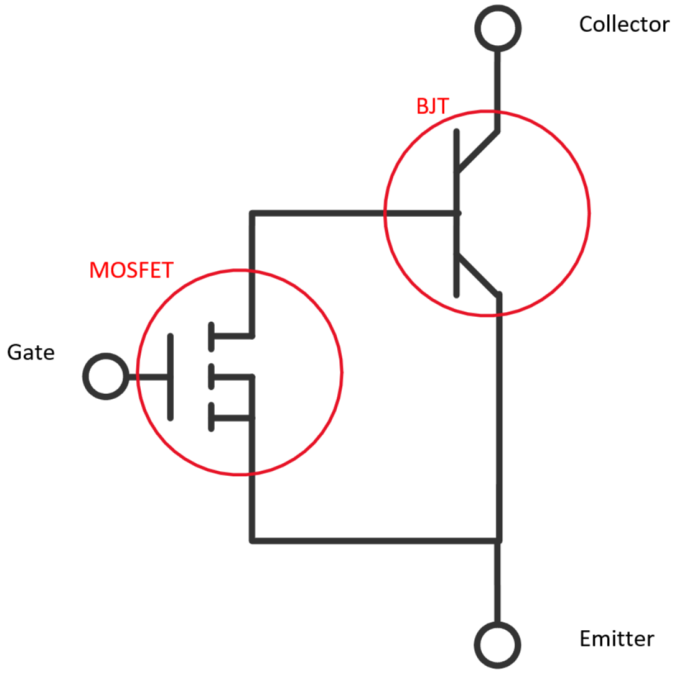

Figure 3.7: IGBT Circuit View

The actual design of the IGBT is shown in Fig.3.8. As would be expected, characteristics of both the MOSFET and the BJT can be seen in the design. The current has to jump straight across some layers as in the BJT, but also must travel across a "capacitance bridge" as in the MOSFET. This combination offers the relay the best of both worlds. The IGBT has the low impedance of the BJT with the low triggering current of the MOSFET. These comparisons can be seen all together in Table 3.1 with data gathered from market products.

Investigating Fig.3.8 more closely helps to show how the current path is formed. The bottom n^+ layer is called the injection layer. This is right next to the collector, or the positive terminal. The next layer, n^- is the drift region. The junction between these two, J1, is set into a forward bias. This sets the junction between the drift

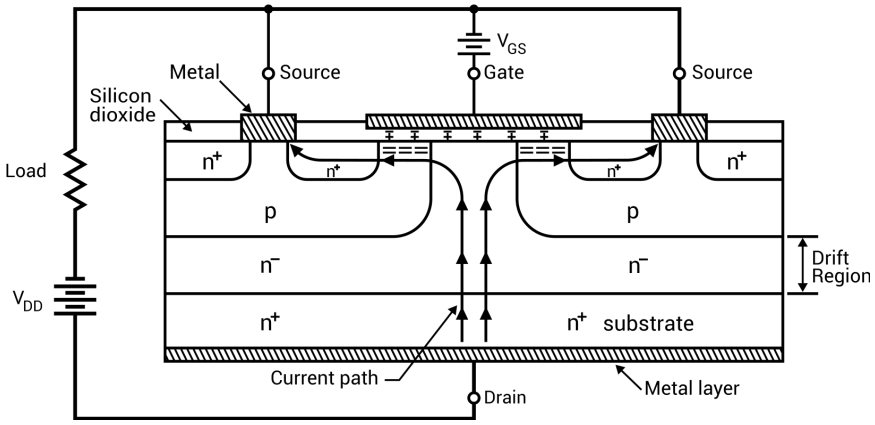

Figure 3.8: IGBT

region and the p-type substrate, J2, to reverse bias. So far, this is the same process observed in the SCR. Now, rather than changing the charge of the whole layer as done in the SCR, a capacitance bridge is formed by the gate allowing the current to flow across the p-type substrate without having to overcome the reverse bias at the entire junction.

3.3 Conclusion

The purpose of this trade study was to determine which of the relays currently available would be most advantageous to the design of the PIT.

Models designed up until the turn of the millenium have all used spark gap switches with gas pressure subsystems and modern larger designs still favor these.(10) Modern designs are now branching out and implementing solid state switches, mostly SCRs.(1) These designs and experiments have been promising, but many concessions had to be made to accommodate these new switches.

The SCR's implemented thus far could not handle the loads required by the larger PIT designs, so the geometry had to be changed. For this reason, modern PIT designs are about one-eighth of the size of the older designs and consequently about one-fourth

Switch Type	SCR	MOSFET	IGBT
Voltage Rating	$\approx 1kV$	$\approx 1kV$	$\approx 6.5kV$
Pulsed Current Rating	$\approx 500A$	$\approx 150A$	$\approx 1.5kA$
Switching Speed	$\approx 10\mu s$	$\approx 100ns$	$\approx 750ns$
Relative Cost	Low	Medium	High

Table 3.1: Solid State Switch Comparison

as efficient.

This study was done in an effort to provide stronger switching options to improve the efficiency of the PIT overall. Given the information above, two designs in particular stand out: IGBTs and thyratrons. The thyratron can handle large power loads and experiences very little damage from erosion. The main drawback is the problem of heat dissipation. To overcome the issue of heat build-up, a heat sink would need to be installed. This would add a significant amount of mass to the thruster overall and the magnitude of the drop in performance would be substantial.

IGBTs seem to have the best fit qualifications out of the solid state relays. They cannot fire as quickly as a MOSFET, but at 750ns, they fire quickly enough for the needs of the thruster. The amount of power they can handle is the highest by a substantial margin. These superior specifications come at a quite literal cost. IGBTs consistently cost approximately 40 times as much as the highest performing SCRs.

Taking all this information into account, the IGBT seems to be the logical option as a replacement for switches in current PIT designs. While they cannot handle the full load required by a 1-m diameter PIT, they can be implemented into a design about half the size. In addition, IGBT designs are constantly being improved. In the last four years alone, market IGBTs have seen a performance increase of 44%.

Chapter 4

IMPROVEMENTS TO PLASMA COUPLING

4.1 Existing Issues

Addressed in this section are two problems found in existing PIT designs: the inefficient device geometry and poor coupling between the accelerator coil and the plasma.

4.1.1 Inefficient Geometry

To understand what is meant by inefficient device geometry, it is important to look at the magentic field being generated. This can be seen in Fig.4.1.(19)

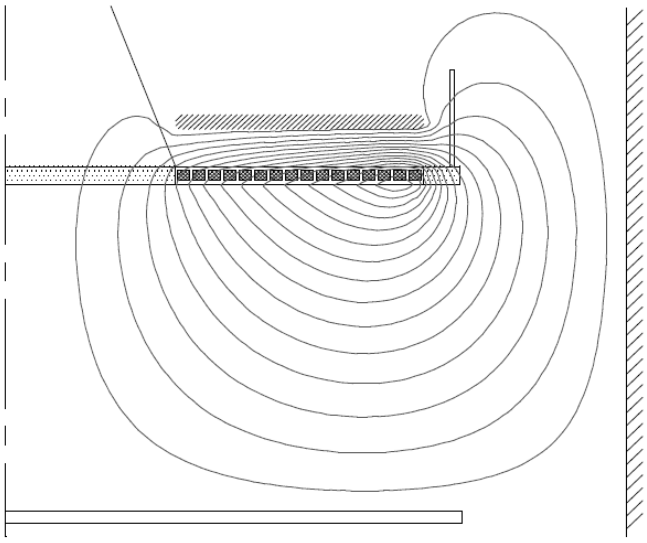

Figure 4.1: Magnetic Field Distribution in the PIT

In the top half of the figure, the magnetic field lines are compressed as they interact with the charged plasma. This compression is desirable as this is what causes the

propellant acceleration. In the bottom half of the figure, the magnetic field reaches down to a length almost half that of the diameter of the coil itself. This magnetic field necessitates a large empty space be designed into the thruster, which increases the mass and volume inherent in the design.

4.1.2 Poor Coupling

As discussed in previous sections, plasma must inductively couple with the accelerator coil before it can be accelerated. The more completely the plasma couples, the more energy can be transferred into the flow.

The problem of poor plasma coupling has been noted in all PIT designs, but most thoroughly investigated in the MkV. In this study, Dailey & Lovberg noted that not all the propellant was being accelerated equally.(10) The propellant gas near the inner and outer radii was not being fully accelerated; in fact, the propellant near the outer wall wasn't being accelerated much at all. Fig.4.2 shows a much higher gas density

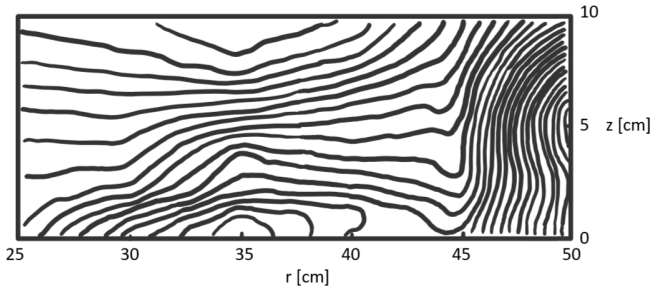

Figure 4.2: Under-Accelerated Propellant

on the outside edge, relative to the area around the rest of the coil after being fired.

4.2 Proposed Solution

4.2.1 Halbach Array

The Halbach array is an arrangement of permanent magnets that manipulates the magnetic field to be stronger on one side of the array than the other. One full pattern of this arrangement requires 5 magnets arranged as shown in Fig.4.3. The polarity of

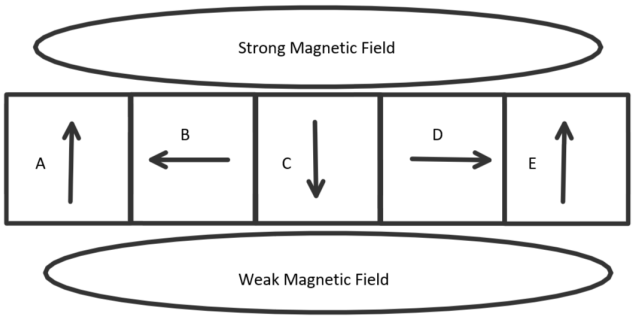

Figure 4.3: Halbach Array Arrangement

each magnet is indicated with the arrow pointing toward the north pole. The center magnet (C) is oriented with the north side facing down, the two adjacent magnets (B and D) have their respective north poles pointing away from the center magnet, and the edge magnets (A and E) are aligned with north pointing up. This results in a magnetic field that is strong above the array, but weak below it. This is why refrigerator magnets usually only stick on one side.

Building a Halbach array is simple, but understanding why it behaves the way it does is a little more complicated and requires a basic understanding of magnetic fields and vector math. Looking at Fig.4.4, the blue loops show the normal, undisturbed magnetic field of each magnet. The Halbach array aligns each magnet so that the individual magnetic fields will interact in such a way as to create a resulting magnetic field (shown in green) that is directional. Magnetic field lines always want to point

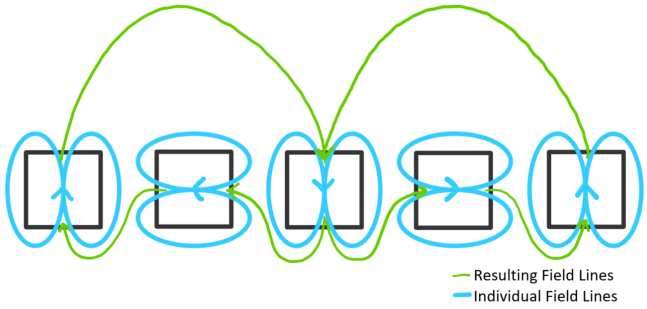

Figure 4.4: Halbach Magnetic Field Lines

in the same direction as the field lines around them. These lines can also never cross other field lines, much like the lines on a topographical map. Following these two rules, it becomes easier to see how the individual blue fields can be used to shape the larger resulting green field.

Before putting a great deal of time and resources into pursuing this design, some proof of concept tests needed to be done to ensure the effect was as strong and beneficial as previous studies had claimed.(17) Using neodymium cube magnets (the black dots represent north) and super glue, a small Halbach array was constructed and can be seen in Fig.4.5. Using magnetic field viewing film, the resulting field lines were made visible. As a result, these lines could be observed to behave precisely as predicted. These results are shown in Fig.4.6.

Adjusting Geometry

The concept of the Halbach array is incredibly useful; however, the geometry does not line up with the geometry of the PIT. Some adjustments to the design had to be made before the Halbach concept could be applied to the PIT. The B and D magnet sections had to be lengthened to better approximate the size of the accelerator coil in the PIT. This geometry is shown in Fig.4.7 and its resulting magnetic field in Fig.4.8.

Figure 4.5: Halbach Array Concept with Permanent Magnets

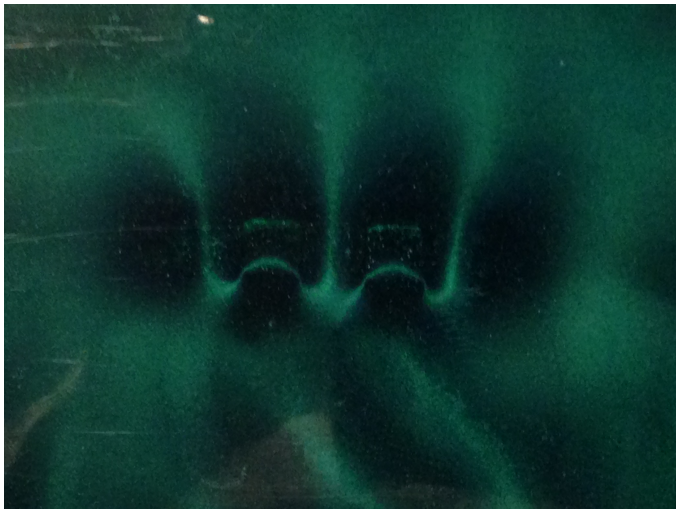

Figure 4.6: Halbach Field with Permanent Magnets

As was expected, the Halbach effect was lessened, but still present.

4.2.2 Modified Halbach Array

Having now shown that the resulting magnetic field could be beneficial to the efficacy of the PIT, work could move forward into methods of implementation. The basic design of an electromagnet is a copper coil wrapped around an iron core. This was the concept used to design the electromagnetic Halbach array and can be seen in

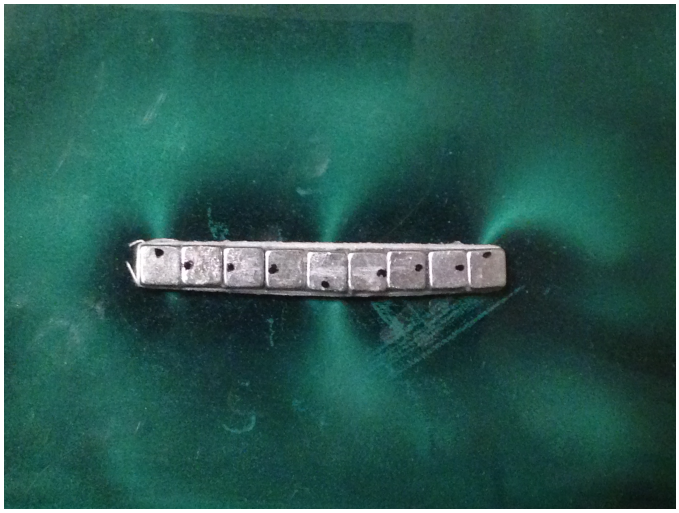

Figure 4.7: Scaled Halbach Array Proof-of-Concept with Permanent Magnets

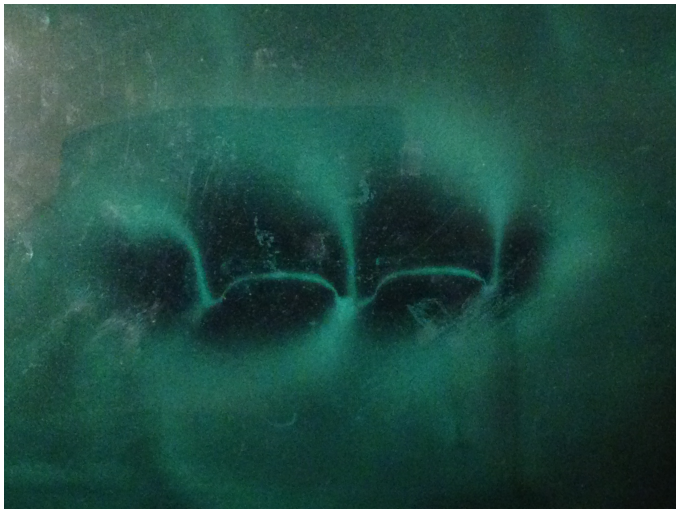

Figure 4.8: Scaled Halbach Field with Permanent Magnets

Fig.4.9. The core has been omitted from this image so all the coils can be seen more easily.

Time and resources wouldn't allow for the actual building and testing of this design, so analysis was done using computer simulation. The coil geometry was imported into FEMM 4.2, a program that analyzes the magnetic fields around physical geometries. The result of running the proposed coil through FEMM can be seen in

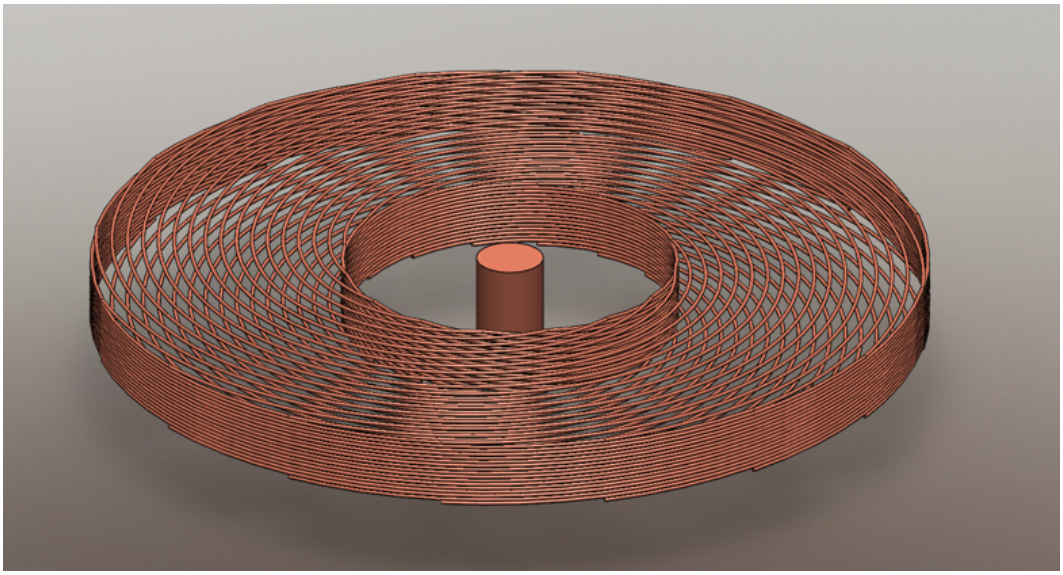

Figure 4.9: Proposed Modified Halbach Array

Fig.4.11. The results from this simulation were promising. The magnetic field below the coil was greatly reduced and the field above and on the edges was improved. These results present potential solutions to the two problems mentioned at the beginning of this section.

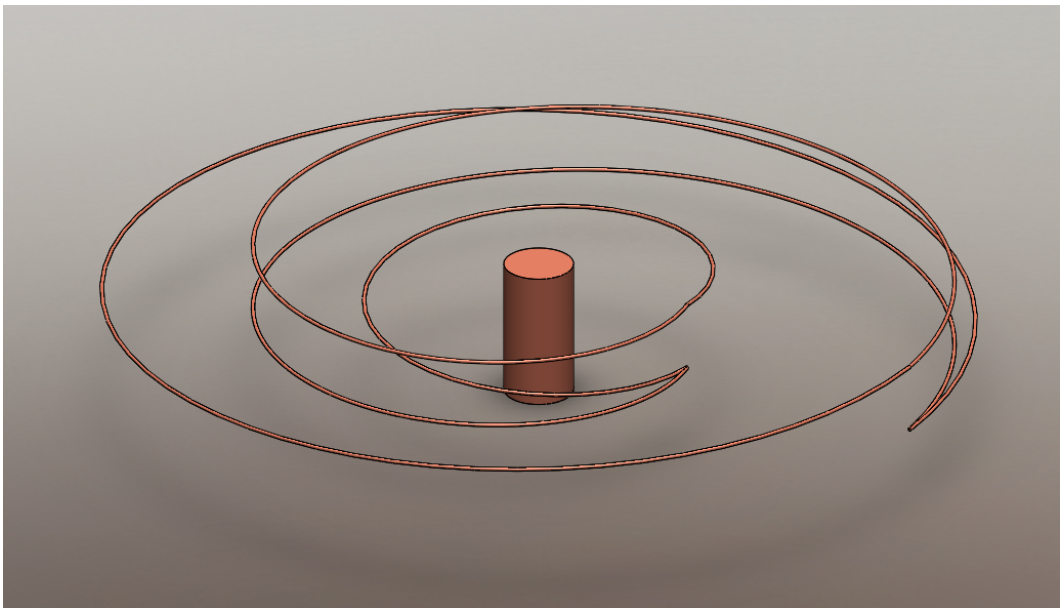

Figure 4.10: Single Coil of the Proposed Modified Halbach Array

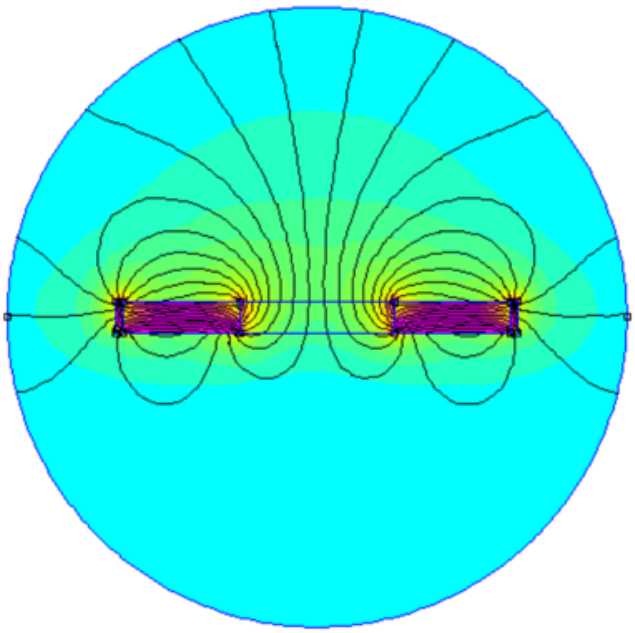

Figure 4.11: Magnetic Field from Proposed Modified Halbach Array

Chapter 5

COMPUTER MODELING

5.1 PIT Simulation

5.1.1 Introduction

This section serves to introduce and explain the MATLAB code written to predict and simulate the performance of a small Pulsed Inductive Thruster (PIT) based on changes made to the electrical circuit and geometry. This simulation utilizes the experimental and theoretical work done by C.L. Dailey & R.H. Lovberg in their design and modeling of PIT's.(6) This model was further modified using advances made at the Marshall Space Flight Center in their work with small Inductive Pulsed Plasma Thrusters (IPPT) and Polzin and Choueiri's research on the FARAD project.(1)(25) With these changes, the simulation should demonstrate results of a higher accuracy than the models upon which it was based. In addition to these improvements, two additional features were implemented into the code. The first feature is that this code is driven by the Alfvén velocity. The second feature is that it can be used to predict the electromagnetic decoupling length.

Nomenclature

M_m	Molecular Mass
eVi	Ionization Potential
N	Number of turn in the coil

C	Capacitance
V	Voltage
E_0	Initial Stored Energy
L_0	External Circuit Inductance
R_e	External Circuit Resistance
u_a	Alfvén Velocity
m_{crit}	Critical Mass
m_{bit}	Mass bit per shot
L_c	Unloaded Coil Inductance
δ_s	Initial Current Sheet Thickness
δ_a	Immediate Current Sheet Thickness
δ_d	Depth of the Propellant Cloud
η	Plasma Resistivity
z_0	Electromagnetic Decoupling Length
r_o	Coil Outer Radius
r_i	Coil Inner Radius
A	Coil Area
dt	Time-Step
t_{max}	Duration of the shot

ψ	Average Critical Resistance Ratio
z	Distance from the Coil
v_z	Propellant Velocity
a_z	Propellant Acceleration
M	Mutual Inductance
I_1	Coil Current
I_2	Plasma Current
m	Entrained Mass
c_ρ	Constants in Computing Gas Density
ρ_a	Propellant Gas Density
R_p	Plasma Resistance

Equations

$$E_0 = \frac{1}{2} C * V^2 \tag{5.1}$$

$$E_{flow} = \frac{1}{2} * m * v_z^2 \tag{5.2}$$

$$E_c oil = \frac{1}{2} * C * V^2 \tag{5.3}$$

$$u_a = \sqrt{\frac{2eVi}{M_m}} \tag{5.4}$$

$$m_{crit} = \frac{2 * E_0}{alv f\acute{e}n^2} \tag{5.5}$$

$$A = \pi * (r_o^2 - r_i^2) \tag{5.6}$$

$$c_{\rho 2} = \frac{2 * m_{bit}}{A * \delta_d} \tag{5.7}$$

$$c_{\rho 1} = 2 * \frac{\frac{m_{bit}}{A} - c_{\rho 2} * \delta_d}{\delta_d^2} \tag{5.8}$$

$$\rho_a = c_{rho1} * z + c_{rho2} \tag{5.9}$$

$$\delta_a = \sqrt{\frac{\eta * t}{\mu_0} + \delta_s^2} \tag{5.10}$$

$$R_p = \frac{\eta * \pi * (r_o + r_i)}{\delta_a * (r_o - r_i)} \tag{5.11}$$

$$\frac{dm}{dt} = A * \frac{dz}{dt} * \int_t^{t+dt} \rho_a dz \tag{5.12}$$

$$\frac{dM}{dt} = -\frac{L_c}{2z_0} * e^{\frac{-z}{2z_0}} * v_z \tag{5.13}$$

$$dI_1 = \frac{V * L_c + (M * I_1 + I_2 * L_c) * \frac{dM}{dt} - I_2 * M * R_p - I_1 * R_e * L_c}{L_c * (L_0 + L_c) - M^2} \tag{5.14}$$

$$\frac{M * \frac{dI_1}{dt} + I_1 * \frac{dM}{dt} - I_2 * R_p}{L_c} \tag{5.15}$$

$$\frac{dV}{dt} = \frac{-I_1}{C} \tag{5.16}$$

$$a_z = \frac{\frac{L_c * I_1^2}{2z_0 * A} * e^{\frac{-z}{z_0}} - \rho_a * v_z^2}{m} \tag{5.17}$$

$$I_{sp} = \frac{v_z}{g_0} \tag{5.18}$$

$$\alpha = \frac{C^2 * V^2 * L_c}{2 * m_{bit} * z_0^2} \tag{5.19}$$

$$v^* = \sqrt{L_0 * C} * \frac{v_z}{z_0} \tag{5.20}$$

$$L^* = \frac{L_0}{L_c} \tag{5.21}$$

$$\eta_t = \frac{m^* * v^{*2}}{2 * L^* * \alpha} \tag{5.22}$$

5.1.2 System Model

Thruster Geometry and Electrical Ciruit

The versatility of this code lies in it's comprehensive customizability. This means that any thruster geometry, firing circuit, or propellant gas can be simulated in any combination. Very little, outside of constants such as gravity, has been hard-coded in.

Plasma Model

The inductively coupled plasma is modeled as a transformer with one coil on the plasma side. This model was originally developed by Dailey & Lovberg in their work on the 1-m thruster in 1979.(6)

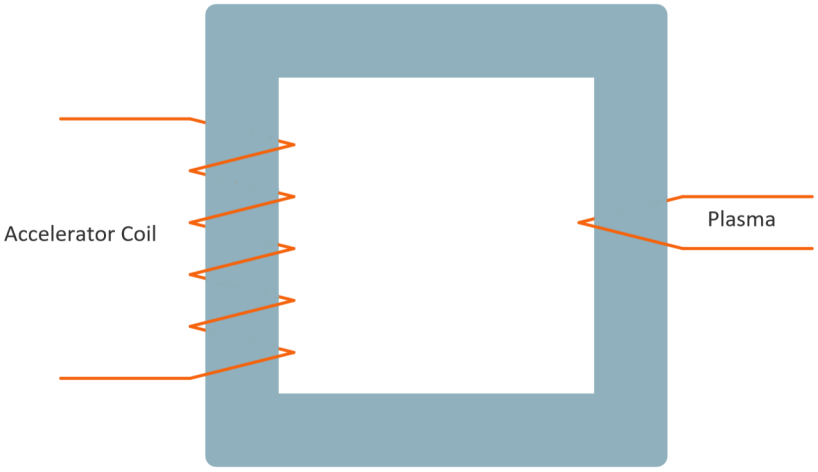

Figure 5.1: Representation of Plasma Coupling as a Transformer

5.1.3 Mass Scaling

The amount of propellant mass that is fed into a thruster can drastically affect the efficiency of the device. There is an optimal amount, or critical mass (m_{crit}), that

should be pumped across the coil to achieve the peak efficiency. Two methods were derived to estimate this m_{crit}. The first method was to create a formula by matching the voltage scaling data found in the MkV paper and scaling that data with the geometry of the thruster relative to the MkV.(10) The resulting relationship is shown in Eq.(5.23).

$$m_{bit}[mg] = ln(-1.6V[kV] - 16.7) \tag{5.23}$$

The second method of calculating the critical mass was done using the Alfvén velocity. The idea is that m_{crit} can be determined theoretically instead of experimentally. The Alfvén velocity can also be used to calculate such parameters as the dynamic impedance parameter α.

$$u_a = \sqrt{\frac{eV_i'}{m_i}} \tag{5.24}$$

$$m_{crit} = \frac{M_m E_0}{eVi'} \tag{5.25}$$

5.1.4 Operation

Inputs

The code has most of the information required to run built in; however, three sets of user inputs are still required. The user must first choose a propellant type. The default in the code is set to pure argon. To choose a propellant, two values must be entered: the molecular mass and the first ionization potential.

The second set of inputs are the characteristics of the users firing circuit. These inputs include bank capacitance, initial charge voltage, external circuit inductance, and external circuit resistance. From these parameters the code computes the total energy initially stored in the circuit. Using the propellant characteristics and the initial energy, the code computes the Alfvén velocity and the critical mass. The critical mass is used as the ideal mass bit.

The third set of inputs are the coil characteristics. The coil size can be set by adjusting the values for the inner and outer diameters. Once the geometry is set, the unloaded coil inductance can be determined.

A guess value for the electromagnetic decoupling length is already set in the code, but this value must be adjusted on subsequent iterations to achieve a realistic efficiency.

Initialization

While the input to the code is a set of scalars, the output of the code is a set of arrays. Each array tracks one characteristic of the thruster with respect to time. Even though most of the parameters start at zero, the code cannot run while all variables are set to zero as this results in an output of empty arrays. Mutual inductance has an initial value equal to the unloaded coil inductance. The initial mass is dependent on the current sheet thickness and the propellant density as the code assumes all propellant is being accelerated. The propellant density is assumed to adhere to a nearly linear model, as shown in Fig. 5.2.

Numerical Analysis

The first step after initialization is to calculate the change in each parameter at the first time step. Most of the values in this code are calculated using a forward in time differential model. As such, the parameters themselves are not calculated at each individual time step, rather the change at that parameter is calculated at each time step and added to the previous value. This is demonstrated in Eq.(5.26).

$$x(i+1) = x(i) + \frac{dx(i)}{dt} * (t(i+1) - t(i)) \tag{5.26}$$

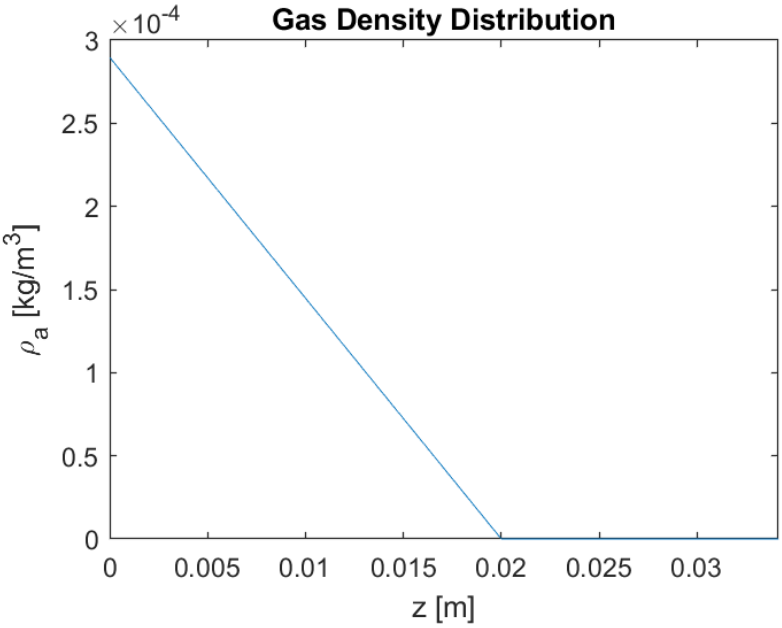

Figure 5.2: Linear Model of the Propellant Distribution with Respect to Distance from the Coil

Following this pattern for each parameter, the code iterates until the plasma has decoupled or until the maximum time has been reached.

Data Analysis

After the the arrays for each parameter have been filled, the code calculates the isp, the dynamic impedance parameter α, and implements a dimensionless analysis to determine the thrust efficiency η_t. This efficiency is checked against the flow and coil energies to ensure all data agrees. This is also the point where the full code can be iterated to improve the estimate for decoupling length.

5.2 Roadblock Discoveries

In this code, as with any program, there were initially typos, calculation errors, and syntax errors to be worked out. However, some issues turned out to be more difficult to understand and resolve. Foremost among these were those involving de-

coupling length and thrust efficiency.

5.2.1 Decoupling Length

Academically, decoupling length is defined as the estimated distance at which the propellant is no longer primarily influenced by the accelerator coil. In practice, however, it is never calculated and must always be determined experimentally. This works reasonably well for most purposes, but it is based on certain assumptions, and these assumptions can be a source of error. For example, in current literature, the assumption is that the decoupling length will remain roughly constant throughout all tests performed on a specific thruster. In fact, the decoupling length is not a set, constant value.

To give an better understanding of the concept, inductive coupling can be compared to gravity. Imagine an isolated system that contains two individual masses. These masses will pull on each other regardless of the distance separating them. In the same manner, two theoretical coils can inductively couple at any distance. In orbital mechanics, the sphere of influence is the three-dimensional space around on object in which it is the primary gravitational influence. This has less to do with the object itself and more to do with it in relation to the objects surrounding it. This sphere of influence is currently how most studies view the decoupling length. However, a more accurate way to look at decoupling would be to compare it to orbital escape velocity. Escape velocity is the speed at which an object must travel to break out of an elliptic orbit and can be achieved at any distance from the gravitational center. As mentioned above, gravity will pull two bodies together regardless of the distance between them, but the magnitude of that pull decreases as distance increases. At escape velocity, the escaping object will constantly be decelerating due to gravity, but the pull of gravity is weakening at an even greater rate. The result of this is that

the escaping object will never decelerate to the point of moving back towards the the pulling body. This is how the decoupling length should be viewed.

The current experimental method for determining decoupling length works quite well, and this code cannot claim to make any improvements to it regarding accuracy as of yet. The current iteration of this code requires cross checking its estimated efficiency values with experimental results and making adjustments based on the discrepancies between the two. All this being said, it is believed that with further interrogation, this method of numerically calculating the decoupling length can lead to a mathematical model that can produce more accurate estimates without the necessity of physical experimentation.

5.2.2 Efficiency Issues

The idea about determining decoupling length came when checking the thrust efficiency (η_t). The code was yielding unrealistic values in the range of 260%, shown in Fig.5.3. As shown in Eq.(5.27), the only values going into the efficiency equation were the mass bit(m_{bit}), the decoupling velocity (v_z), the bank capacitance (C_B), and the stored voltage (V).

$$\eta_t = \frac{\frac{1}{2} m_{bit} v_z^2}{\frac{1}{2} C_B V^2} \tag{5.27}$$

To try and find the error, it was necessary to step back through the algorithm, starting from the efficiency. The voltage and capacitance are set by the circuit and the mass bit is determined using the Alfvén velocity, so the issue had to lie in the velocity. Velocity is driven by a hard-coded time-step and the acceleration. The value for the acceleration is determined by Eq.(5.28)

$$a_z = \frac{\frac{L_c * I_1^2}{2 * z_0 * A} * e^{\frac{-z}{z_0}} - \rho_a * v_z^2}{m} \tag{5.28}$$

Taking this same strategy, tracking back all the way leads to equations (5.28) and (5.29).

$$\frac{\partial M}{\partial t} = -\frac{L_c}{2z_0} * e^{\frac{-z}{2z_0}} * v_z \tag{5.29}$$

The two common hard-coded variables in these two equations were the unloaded coil inductance (L_c) and the decoupling length (z_0). L_c is dependent on the coil geometry and was experimentally determined but z_0 had just been a guess based on previous work. Previously it had been assumed that the decoupling length would scale with the thrusters geometry, but this proved to be incorrect as it must also reflect the energy put into the system.

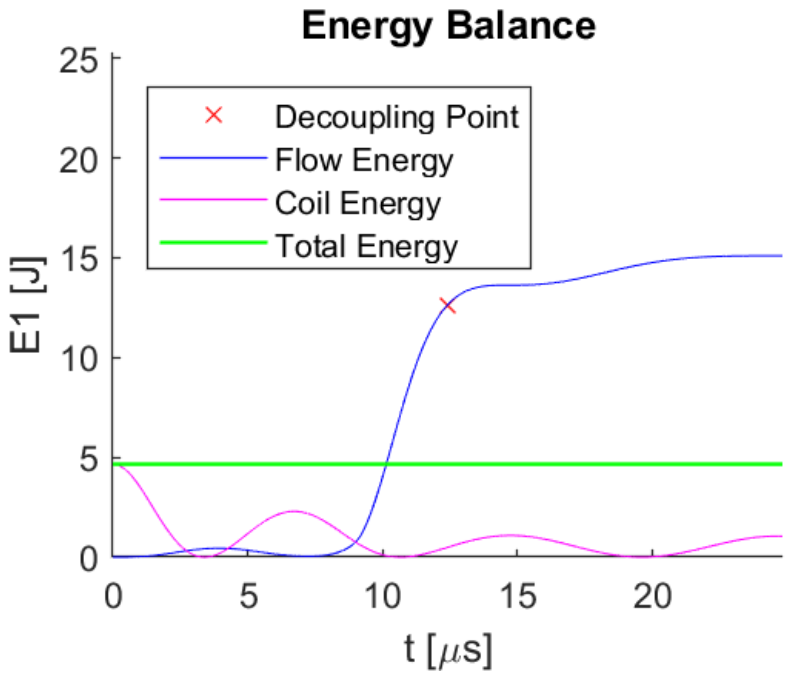

Figure 5.3: Unrealistic Energy Balance Due to Fixed Decoupling Length

5.3 Conservation of Energy

While attempting to discover the source of the efficiency errors mentioned above, it was noted that the previous models, those upon which this work has been based,

contained the same root deficiency. None of the predictive PIT models directly accounted for the conservation of energy. In most of these models, this issue was not apparent as the thrust efficiency never exceeded 100%. This is most likely due to the fact that much of the input data in these models had been obtained experimentally.

Without the aid of these experiments, these models would likely be far less accurate and less useful as predictive tools. To truly simulate the behavior of a PIT, conservation of energy must be included as one of the governing equations.

To further demonstrate this concept, poorly optimized test parameters were entered into the PIT model. Without accounting for conservation of energy, the data was smooth and displayed the proper trends. The resulting energy balance is shown in Fig.5.3. While it looks good, it is clear that the result shown is impossible as the energy transferred to the flow is far greater than the initial energy stored in the capacitor bank. The test was run again, but this time the model was forced to conserve energy. The resulting energy balance of this test is shown in Fig.5.14. This plot is bumpy and does not seem to behave how an operating PIT should, but the flow energy never exceeds the initial stored energy. These two characteristics, conservation of energy and the "prettiness" of the plotted data, offer credence to the hypothesis the PIT predictive models are lacking on a fundamental level. This test was designed using poorly optimized input parameters, as a result, the output data should be equally poor. Put another way, testing a poorly designed thruster should result in poor performance characteristics, and that is exactly what is seen in Fig.5.14.

5.4 Results for Desired PIT Design

At the onset of this project, physical tests were designed to compare with the results of the code. Because hardware suppliers were unable to deliver materials in a timely manner, these test rigs could not be built and tested. Even though physical

testing was not an option, these design parameters were still tested in the code and run on an ideal case of total energy conversion. These results can be seen in Fig.5.4 -Fig.5.14. Even at 100% efficiency, this thruster could only achieve an *isp* of 820.49s. This was much lower than the expected outcome of 1500s at 30%. The poor design can also be seen in the jagged curves shown in the figures. In this design, the plasma cannot accelerate away before the current reverses in the accelerator coil and pulls it back.

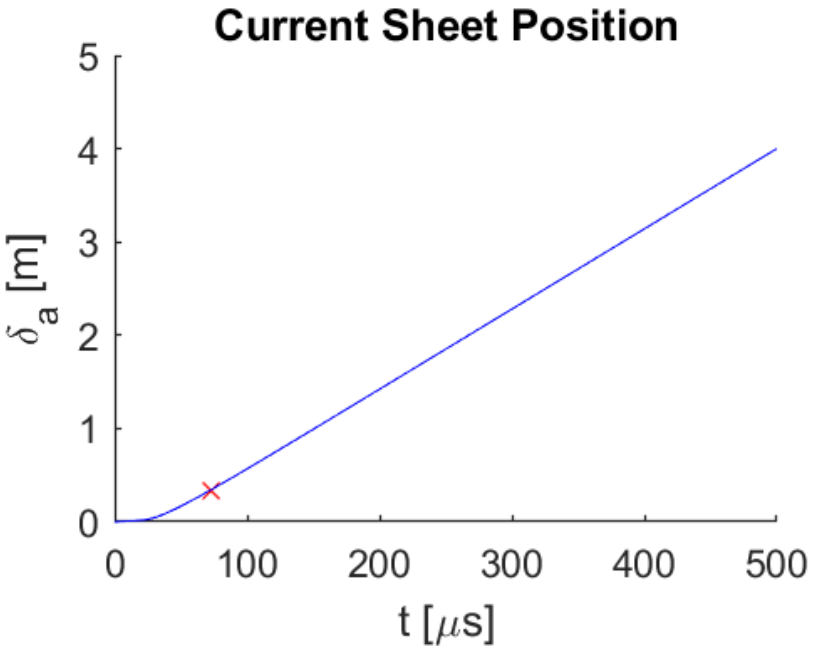

Figure 5.4: Current Sheet Position at 100% Energy Conversion

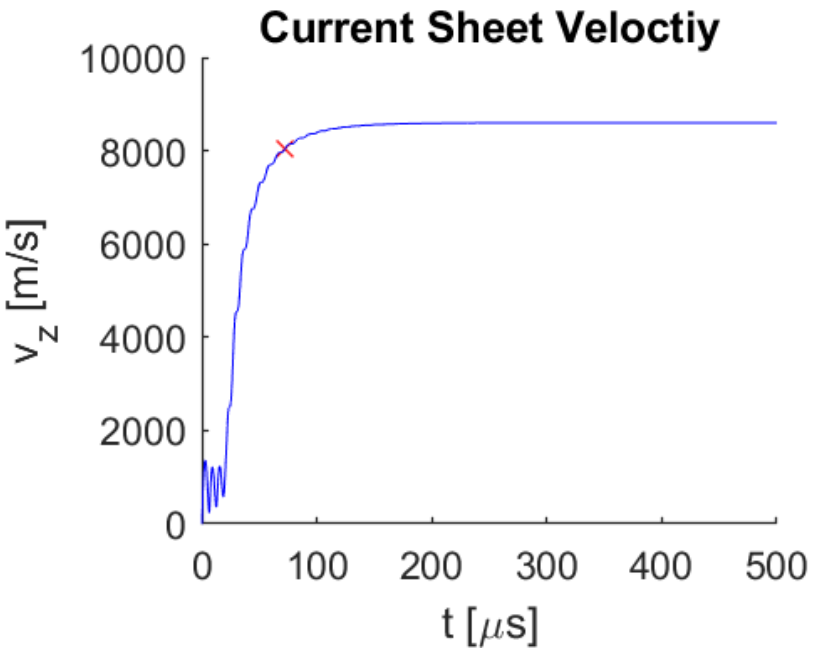

Figure 5.5: Current Sheet Velocity at 100% Energy Conversion

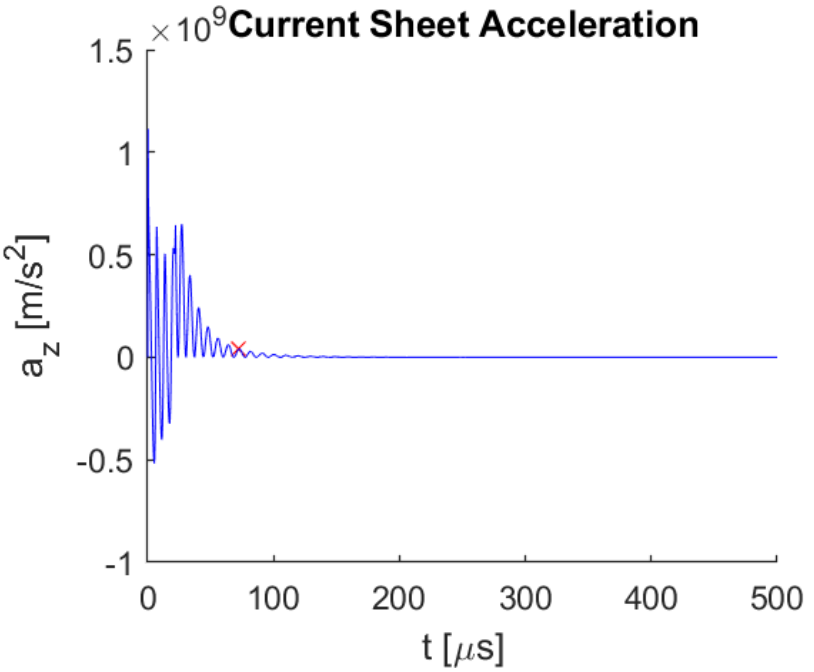

Figure 5.6: Current Sheet Acceleration at 100% Energy Conversion

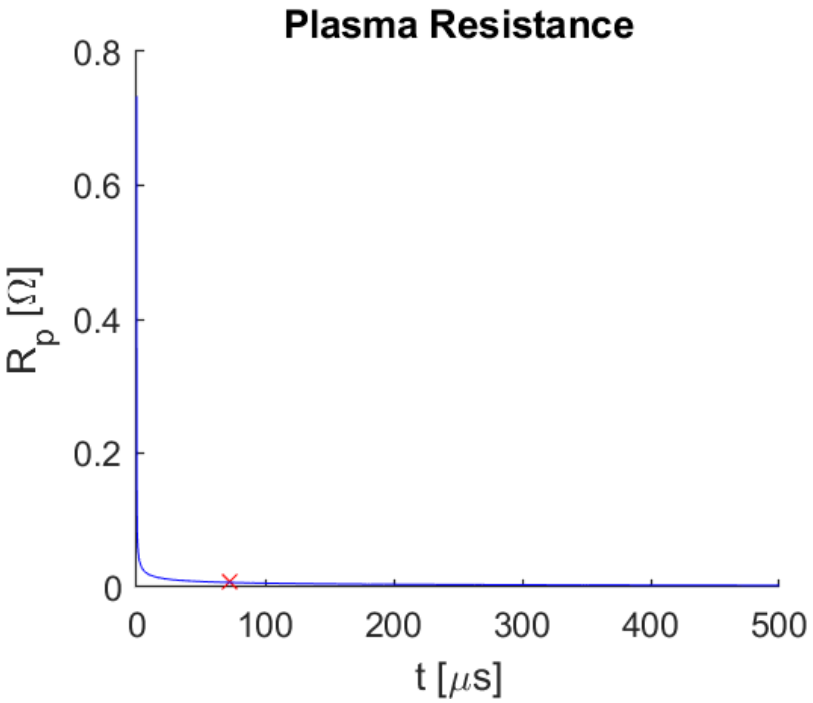

Figure 5.7: Plasma Resistance at 100% Energy Conversion

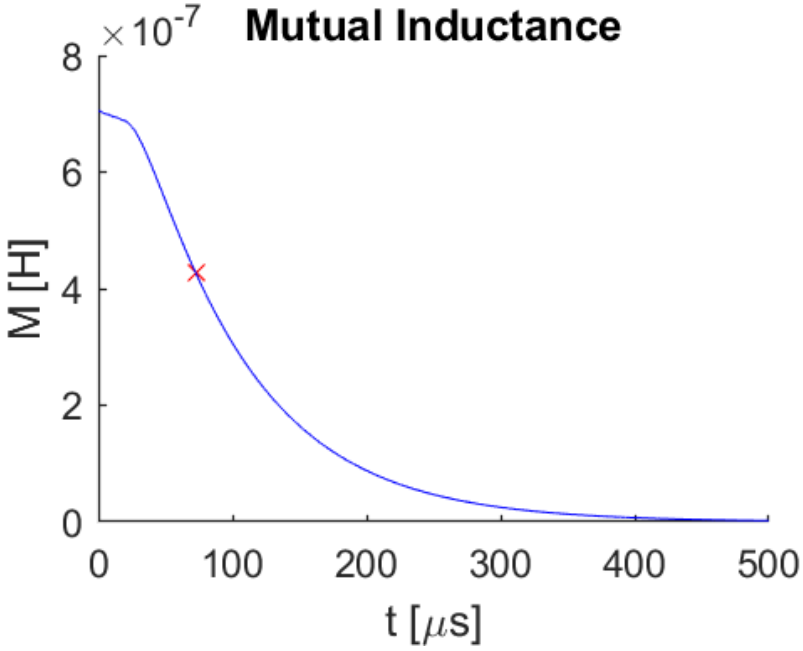

Figure 5.8: Mutual Inductance at 100% Energy Conversion

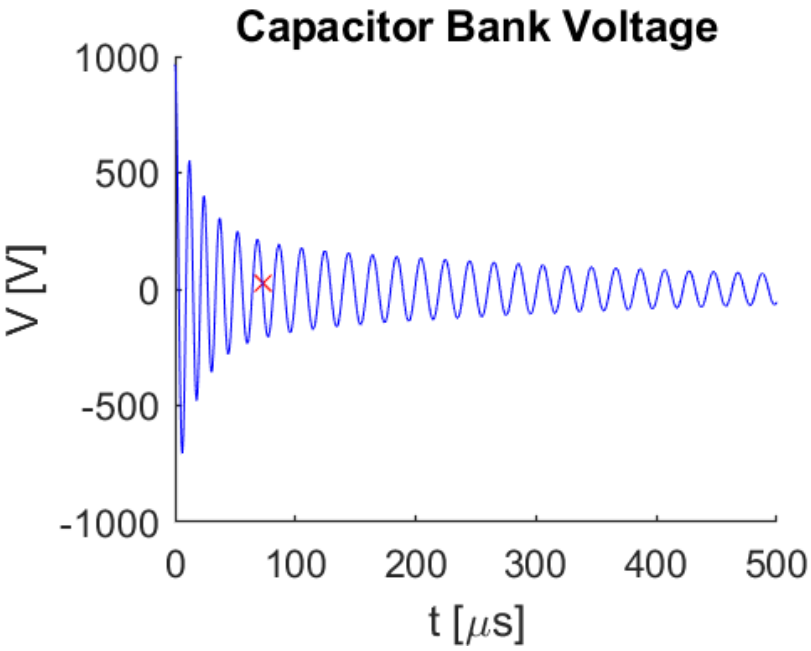

Figure 5.9: Capacitor Bank Voltage at 100% Energy Conversion

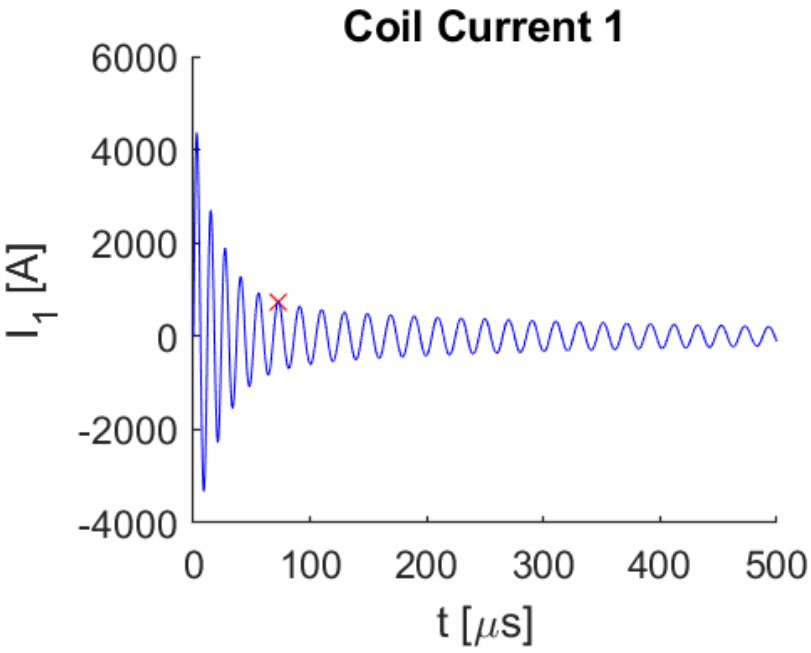

Figure 5.10: Coil Current at 100% Energy Conversion

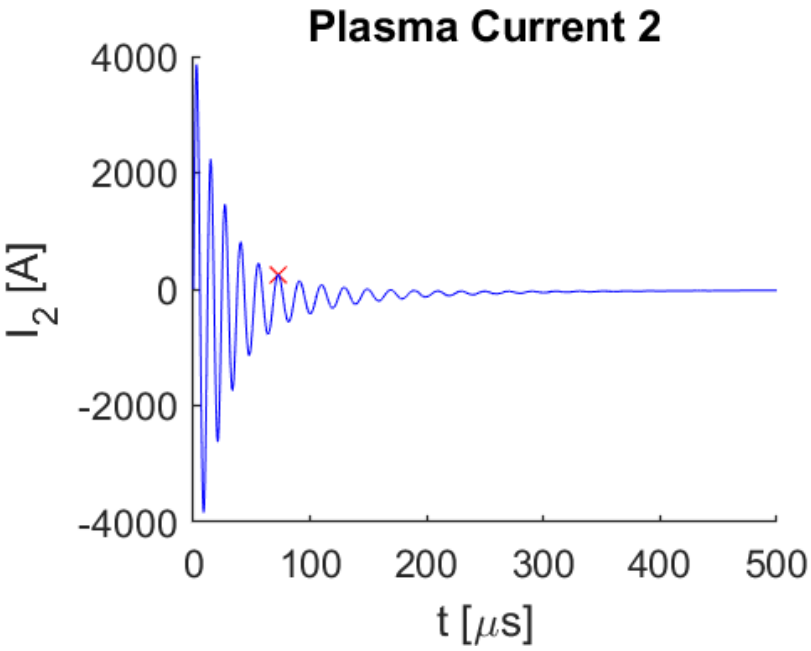

Figure 5.11: Plasma Current at 100% Energy Conversion

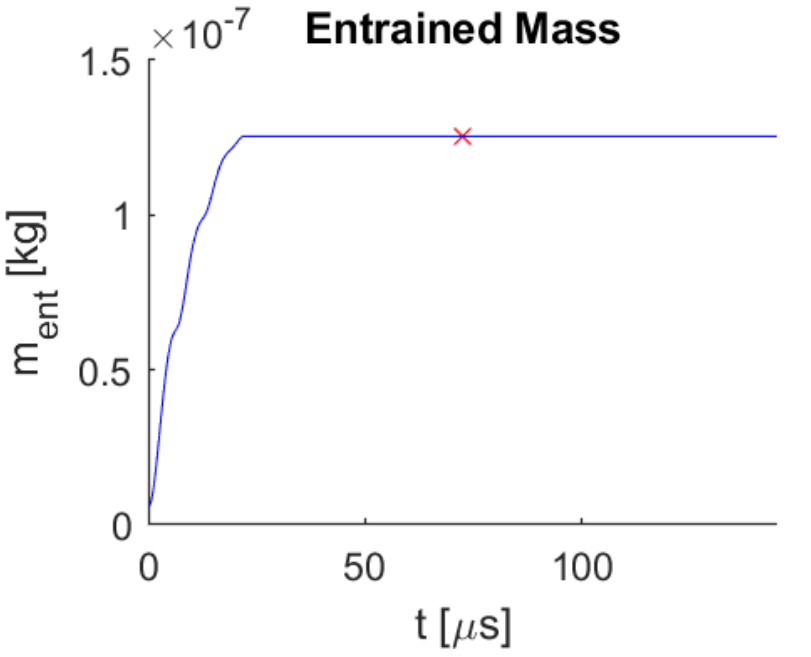

Figure 5.12: Entrained Mass at 100% Energy Conversion

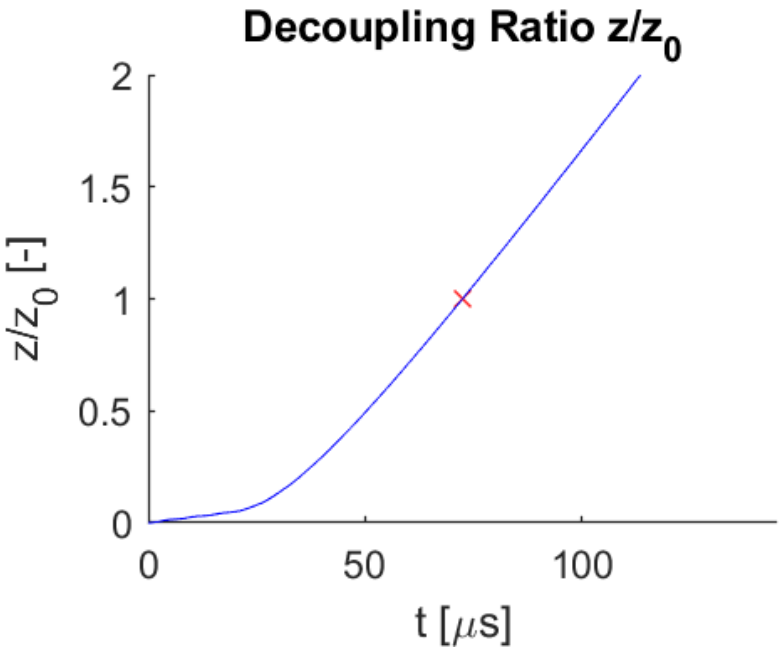

Figure 5.13: Decoupling Ratio at 100% Energy Conversion

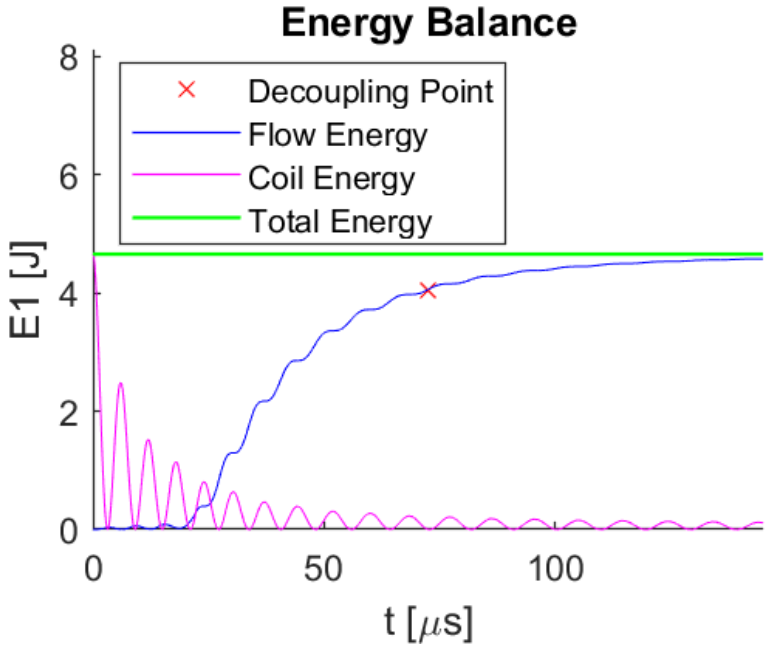

Figure 5.14: Distribution of Energy at 100% Energy Conversion

Chapter 6

CONCLUSION

Three major studies have been presented in this work: the triggering circuit relay trade study, the proposal of a modified coil geometry to improve plasma coupling, and the computer model used to simulate a single shot in PIT operation. This work was done to demonstrate the potential of PITs and encourage future work to be aimed in that direction.

6.1 Computer Modeling

6.1.1 Conclusion

In relation to predicting the decoupling length, the code written seems to produce believable values for the parameters that are fed into it. It can be used to approximate the results of past studies, if not recreate them exactly. The output values were accurate enough that trends could be followed. This allowed for some confidence in analyzing thruster designs for which there is no published data.

In analyzing these untested geometries, some ad hoc modifications were made to the code to enforce the conservation of energy. Similar modifications have not been previously implemented in other predictive models of this nature; consequently, it is difficult to determine the increase in quality of the output data.

As mentioned previously, in relation to predicting the decoupling length, no claims are made that the code in it's current state can provide a greater amount of accuracy than experimental data. However, this code represents the early stages of a new method of analyzing inductively coupled plasmas which could, in subsequent versions, provide a great deal of accuracy and offer some insight into plasma dynamics.

6.1.2 Future Work

Not included in this work is a matlab code designed to simulate fluid flow in two dimensions. This code was not written with this project in mind, but it could be easily implemented. The goal of this would be to move away from the linear gas density model currently being employed. This would be implemented as a backward in time, upwind scheme. This addition, more than anything, would remove errors inherent in the gas distribution assumption and greatly increase the accuracy of the model.

6.2 Triggering Circuit

6.2.1 Conclusion

Most published research in this area has been done using thyristors. As shown in this study, thyristors are a strong candidate for use as the switches in PIT triggering circuits; however, IGBTs currently available show much greater promise as they can switch much faster and handle greater peak current values at comparable impedance values. They are the most expensive switch available, but not to the point of being cost prohibitive.

6.2.2 Future Work

One method of implementing solid state switches that was not mentioned in this study was preionization. Preionization is not a new or revolutionary concept, it was used extensively in the work done by Dailey & Lovberg in the 70's.(11). It is, however, an underutilized tool. In conventional PITs, a portion of the charge on the acceleration coil is used to fully ionize the propellant and the remaining charge is used to accelerate it away. If the propellant were already ionized upon reaching the

coil, the coil would only need to be charged for that fraction of the voltage used in the acceleration mechanism. Some resaerch has already explored this concept. In the FARAD project at Princeton,(25) Polzin & Choueiri have had promising results using an RF-discharge stage as the preionizer.

6.3 Modified Acceleration Coil

6.3.1 Conclusion

All simulations showed the desired magnetic field distribution was achieved through the use of the modified Halbach array. This presents the possibility of a more compact and more efficient thruster design. While these results are promising, this study was not a comprehensive operational analysis. There are aspects of this design that must be considered before implementation. The coil geometry is far more complex and requires more coil length which adds mass to the system. It is unknown whether the mass added would be proportional to the efficiency gained. If the specific mass were to increase with the implementation of this design, it would not serve its intended purpose. The above-mentioned complexity is also a major issue to overcome. With the amount of power pushed through each coil, they tend to heat up to dangerous levels. For this reason, coils are often made from copper pipes and a cooling liquid is pumped through them. With the complexity of the modified Halbach array, the flow of the cooling liquid would be impeded at several junctions. In addition to this, the increased length of the coil would require more cooling liquid, increasing the mass of the spacecraft.

6.3.2 Future Work

This design was put together purely as a simulated proof of concept. It is in its most basic form, and very little E-M field analysis has been done beyond analysis of the existing design. Rather than design the coil in the hope that it will produce a favorable magnetic field, future analysis should work the other way. That is, in depth magnetic field analysis should drive the development of the coil geometry.

REFERENCES

[1] *Design and Testing of a Small Inductive Pulsed Plasma Thruster* (International Electric Propulsion Conference, Kobe-Hyogo, Japan, 2015).

[2] Alfven, H., "Existence of electromagnetic-hydrodynamic waves", Nature **150**, 3805, 405–406 (1942).

[3] Baliga, B., "Enhancement and depletion mode vertical channel m.o.s. gated thyristors", Electronics Letters p. 645 (1979).

[4] Bilstein, R., *Stages to Saturn: A Technological History of the Apollo/Saturn Launch Vehicle* (DIANE Publishing, Pensylvania, 1999).

[5] Dailey, C., "Plasma properties in an inductive pulsed plasma accelerator", Proceedings of the 6th Biennial AIAA/Northwestern University Gas Dynamics Symposium (1965).

[6] Dailey, C. and R. Lovberg, "Large diameter inductive plasma thrusters", Electric proopulsion and its application to space missions (1979).

[7] Dailey, C. L. and H. Davis, "Pulsed plasma propulsion technology", Tech. rep., TRW, Redondo Beach (1973).

[8] Dailey, C. L. and R. Lovberg, "Pit clamped discharge evolution", Tech. rep., TRW, Redondo Beach (1988).

[9] Dailey, C. L. and R. Lovberg, "Current sheet development in a pulsed inductive accelerator", Tech. rep., TRW, Redondo Beach (1989).

[10] Dailey, C. L. and R. Lovberg, "The pit mkv pulsed inductive thruster", Tech. rep., TRW, Redondo Beach (1993).

[11] Dailey, C. L. and R. H. Lovberg, "Current sheet structure in an inductive-impulsive plasma accelerator", AIAA Journal **10**, 2, 125–129 (1972).

[12] Funaki, I. and S. Iihara, "Hall thruster system design for high delta-v missions", Tech. rep., JAXA (2015).

[13] Goldstein, S. A. and R. Lee, "Ion-induced pinch and the enhancement of ion current by pinched electron flow in relativistic diodes", Physical Review Letters **35**, 16 (1975).

[14] Havanur, S., "Power mosfet basics - understanding voltage ratings", Tech. rep., Vishay Siliconix, Santa Clara (2017).

[15] Hubert, C., *Electric Circuits AC/DC: An Integrated Approach* (McGraw-Hill, New York, 1982).

[16] Jahn, R. G., *Physics of Electric Propulsion* (McGraw-Hill, New York, 1968).

[17] Lijesh, K. P. and H. Hirani, "Design and development of halbach electromagnet for active magnetic bearing", Progress in Electromagnetics Research **56**, 173–181 (2015).

[18] Lovberg, R., "Investigation of current microstructure", AIAA Journal **4**, 7, 1215–1222 (1966).

[19] Lovberg, R. and C. Dailey, "Pit primer", Tech. rep., TRW, Redondo Beach (1993).

[20] Martin, A. and R. Eskridge, "Electrical coupling efficiency of inductive plasma accelerators", Journal of Physics D: Applied Physics **38**, 4168–4179 (2005).

[21] Marx, E., "Experiments on the testing of insulators using high voltage pulses", Elektrotechnische Zeitschrift (1924).

[22] Mims-III, F. M., *Getting Started in Electronics* (Master Publishing, Illinois, 1983).

[23] Pirrie, C. and H. Menown, "The evolution of the hydrogen thyratron", Conference Record of the 2000 Twenty-fourth International Power Modulator Symposium pp. 9–16 (2000).

[24] Polzin, K., "Scaling and systems considerations in pulsed inductive plasma thrusters", IEEE Transactions on Plasma Science **36**, 5, 2189–2198 (2008).

[25] Polzin, K. A., *Faraday Accelerator with Radio-frequency Assisted Discharge*, Ph.D. thesis, Princeton (2006).

[26] Polzin, K. A., "Comprehensive review of planar pulsed inductive plasma thruster research and technology", Journal of Propulsion and Power **27**, 3 (2011).

[27] Pugh, M. H., "Spark gap electrode erosion", Tech. rep., Texas Tech. University, Lubbock (1984).

[28] Spitzer, L., *Physics of Fully Ionized Gases* (Interscience, 1956).

[29] Sutton, G. P., *Rocket Propulsion Elements* (John Wiley & Sons, New Jersey, 2010).

[30] Szabo, J., "Generalized ohm's law in a magnetic plasma", Beitrage aus der Plasmaphysik **5**, 9–12 (1965).

[31] Toftul, A., K. Polzin, A. Martin and J. Hudgens, "Testing of diode-clamping in an inductive pulsed plasma thruster circuit", Conference Record of the 50th AIAA Joint Propulsion Conference (2014).

[32] Wendt, Z., "Solid state vs. electromechanical relays", Arrow (2017).

[33] White, D., "Lecture notes in mae 598: Space propulsion", (2017).

APPENDIX A

MATLAB CODE

```
% Taylor Raines
% 1204821653
% Thesis
% PIT Simulation
% Updated: Feb 13, 2018

clc; clearvars; close all;
addOns;
format compact;

%% Add-ons
% Thesis Add-ons

% Constants
-------------------------------------------------------------------

% Gravity
g=9.807;                % m/s^2
% Vacuum Permeabiility
mu0 = 4*pi*1e-7;        % H/m


% Display Options
screensize=get(groot,'Screensize');
dual=1;       % Dual monitor switch
xx=dual*screensize(3);
yy=screensize(4);
figdim=xx/(dual*4);

%% Initialize
% Input Parameters - - - - - - - - - - - - - - - - - - - - - - - -
    - - - - - - -

% Material - - - - - - - - - - - - - - - - - - - - - - - - - - -
% Argon
% Molecular Mass
Mm=0.039;                   % kg/mol
% Ionization Potential
eVi=15.76;                  % eV/atom
eVi=eVi*96487.84;           % J/mol

% Bank Parameters - - - - - - - - - - - - - - - - - - - - - - -
% Number of turns (1979 paper)
N=1;
% Capacitance
C=(N^2)*10e-6;          % F
% Test capictor limited to 10 microF but 100 yields better
```

```
    numerical
% results.
% Initial Charge Voltage
Volt=965;                   % V
% Initial Stored Energy
E0=0.5*C*Volt^2;
% External Circuit Inductance
L0 = (336e-9)/(N^2);          % H
% External Circuit Resistance
Re = 0.005/(N^2);             % Ohms


% Alfven Velocity
alfven=sqrt(2*eVi/Mm);
% Critical Mass
m_crit=2*E0/(alfven^2);
% Mass Bit per Shot
mbit=m_crit;                % kg
% mbit=2e-8;
% Unloaded Coil Inductance
Lc = 705e-9;            % H
% Initial Current Sheet Thickness
ds = 5.0e-4;            % m
% Plasma Depth
dd=0.02;                % m
% Plasma Resistivity
eta = 5e-5;             % Ohm-m
% Electromagnetic Decoupling Length
z0 = 0.3415;             % m
% Coil Outer Radius
r_o = 0.25/2;           % m
% Coil Inner Radius
r_i = 0.1/2;            % m
% Coil Area
A = pi*(r_o^2-r_i^2); % m^2
% Time-Step
dt = 1e-9;              % s
% Time Duration
tmax=500e-6;              % s (1.92e-6)

% Dynamic Impedance Parameter
% alpha=3;
% Average Critical Resistance Ratio
psi=0.9;

%% Initialize Matrices
tsize=round(tmax/dt+1);
```

```
z=zeros(tsize,1);
vz=zeros(tsize,1);
az=zeros(tsize,1);
dM=zeros(tsize,1);
M=zeros(tsize,1);
dI1=zeros(tsize,1);
I1=zeros(tsize,1);
dI2=zeros(tsize,1);
I2=zeros(tsize,1);
m=zeros(tsize,1);
dV=zeros(tsize,1);
V=zeros(tsize,1);
da=zeros(tsize,1);
Rp=zeros(tsize,1);
rhoa=zeros(tsize,1);
T=zeros(tsize,1);

T(1) = 0;          % s
I1(1) = 0;         % Amps
I2(1) = 0;         % Amps
M(1) = Lc;         % H
z(1) = 0;          % m
vz(1) = 0;         % m/s

%% Equations
c_rho2=2*mbit/(A*dd);
c_rho1=2*((mbit/A)-c_rho2*dd)/(dd^2);

% Current Sheet Thickness
da(1) = sqrt(eta*T(1)/mu0+ds^2);
% Plasma Resistance
Rp(1) = eta*pi*(r_o+r_i)/(da(1)*(r_o-r_i));
% Plasma Density
rhoa(1)=c_rho1*z(1)+c_rho2;
% Entrained Mass
m0=A*(c_rho1*(ds^2)/2+c_rho2*ds);
m(1) = m0;
% Equivalent Circuit Capacitance
% C=L0*(24/(Re+Rp(1)))^2;                          % F

% Capacitor Voltage
% V(1)=sqrt(2*alpha*mbit*(z0^2)/(C*Lc));     % V
V(1)=Volt;                                          % V-max for our
    setup
% Change in Mutual Inductance
dM(1) = -(Lc/(2*z0))*exp(-z(1)/(2*z0))*vz(1);
% Change in Circuit Current
```

```
137 dI1(1) = (V(1)*Lc+(M(1)*I1(1)+I2(1)*Lc)*dM(1)-I2(1)*M(1)*Rp
        (1)-I1(1)*Re*Lc)/(Lc*(L0+Lc)-M(1)^2);
138 % Change in Plasma Current
139 dI2(1) = (M(1)*dI1(1)+I1(1)*dM(1)-I2(1)*Rp(1))/Lc;
140 % Change in Capacitor Voltage
141 dV(1) = -I1(1)/C;
142 % Plasma Sheet Acceleration
143 az(1) = ((Lc*I1(1)^2)/(2*z0*A)*exp(-z(1)/z0)-rhoa(1)*vz(1)^2)
        /m(1);
144
145 i=1;
146 z_check=1;
147 for t=dt:dt:tmax
148     i = i+1;
149
150     I1(i) = I1(i-1)+dI1(i-1)*dt;
151     I2(i) = I2(i-1)+dI2(i-1)*dt;
152     V(i) = V(i-1)+dV(i-1)*dt;
153     z(i) = z(i-1)+vz(i-1)*dt;
154     M(i) = Lc*exp(-z(i)/(2*z0));
155     vz(i) = vz(i-1)+1*az(i-1)*dt;
156     da(i) = sqrt(eta*t/mu0+ds^2);
157     Rp(i) = eta*pi*(r_o+r_i)/(da(i)*(r_o-r_i));
158
159     if z(i)<dd
160         rhoa(i)=(c_rho1)*z(i)+c_rho2;
161     else
162         rhoa(i)=0;
163     end
164
165     if z(i)<dd
166         m(i) = m(i-1)+A*(((c_rho1*z(i)^2)/2+c_rho2*z(i))...
167             -((c_rho1*z(i-1)^2)/2+c_rho2*z(i-1)));
168     else
169         m(i) = m(i-1);
170     end
171     dM(i) = -(Lc/(2*z0))*exp(-z(i)/(2*z0))*vz(i);
172     dI1(i) = (V(i)*Lc+(M(i)*I1(i)+I2(i)*Lc)*dM(i)-I2(i)*M(i)*
        Rp(i)-I1(i)*Re*Lc)/(Lc*(L0+Lc)-M(i)^2);
173     dI2(i) = (M(i)*dI1(i)+I1(i)*dM(i)-I2(i)*Rp(i))/Lc;
174     dV(i) = -1*I1(i)/(C);
175     az(i) = ((Lc*I1(i)^2)/(2*z0*A)*exp(-z(i)/z0)-rhoa(i)*vz(i
        )^2)/m(i);
176     if z(i)>z0 && z_check==1
177         z_check=0;
178         decouple=i;
179     end
```

```
180
181 end
182 % decouple=i;
183 %% Analysis
184 % Specific Impulse
185 isp=vz(decouple)/g;
186 % Decoupling Ratio z/z0
187 z_z0=z./z0;
188 % Dynamic Impedance Parameter
189 alpha=((C^2)*(V(1)^2)*Lc)/(2*mbit*z0^2);
190 % Thruster Efficiency
191 m_star=1;
192 vz_star=sqrt(L0*C)*vz(decouple)/z0;
193 L_star=L0/Lc;
194 eta_thrust=m_star*(vz_star^2)/(2*L_star*alpha);
195
196 % Tracking Energy
197 E_flow=.5.*m.*vz.^2;
198 E1=.5*C.*V.^2;
199 % E2=(I2.^2).*Rp*dt;
200 % Use this to find the decoupling length that gives a perfect
      energy
201 % conversion from the coil to the jet kinetic energy
202 %% Plot
203 showplots=1;
204 if showplots==1
205
206 t=0:dt:tmax;
207 figure('name','Current Sheet Position','outerposition',[xx-4*
      figdim yy-1*figdim figdim figdim])
208 hold on
209 plot(t(decouple)*1e6,z(decouple), 'x','color', [1 0 0])
210 plot(t*1e6,z,'color', [0 0 1])
211 title('Current Sheet Position')
212 xlabel('t [\mus]')
213 ylabel('\delta_a [m]')
214
215 figure('name','Current Sheet Velocity','outerposition',[xx-3*
      figdim yy-1*figdim figdim figdim])
216 hold on
217 plot(t(decouple)*1e6,vz(decouple), 'x','color', [1 0 0])
218 plot(t*1e6,vz,'color', [0 0 1])
219 title('Current Sheet Veloctiy')
220 xlabel('t [\mus]')
221 ylabel('v_z [m/s]')
222
223 figure('name','Current Sheet Acceleration','outerposition',[
```

```
    xx-2*figdim yy-1*figdim figdim figdim])
hold on
plot(t(decouple)*1e6,az(decouple), 'x','color', [1 0 0])
plot(t*1e6,az,'color', [0 0 1])
title('Current Sheet Acceleration')
xlabel('t [\mus]')
ylabel('a_z [m/s^2]')

figure('name','Plasma Resistance','outerposition',[xx-1*
    figdim yy-1*figdim figdim figdim])
hold on
plot(t(decouple)*1e6,Rp(decouple), 'x','color', [1 0 0])
plot(t*1e6,Rp,'color', [0 0 1])
title('Plasma Resistance')
xlabel('t [\mus]')
ylabel('R_p [\Omega]')

figure('name','Mutual Inductance','outerposition',[xx-4*
    figdim yy-2*figdim figdim figdim])
hold on
plot(t(decouple)*1e6,M(decouple), 'x','color', [1 0 0])
plot(t*1e6,M,'color', [0 0 1])
title('Mutual Inductance')
xlabel('t [\mus]')
ylabel('M [H]')

figure('name','Capacitor Bank Voltage','outerposition',[xx-3*
    figdim yy-2*figdim figdim figdim])
hold on
plot(t(decouple)*1e6,V(decouple), 'x','color', [1 0 0])
plot(t*1e6,V,'color', [0 0 1])
title('Capacitor Bank Voltage')
xlabel('t [\mus]')
ylabel('V [V]')

figure('name','Coil Current 1','outerposition',[xx-2*figdim
    yy-2*figdim figdim figdim])
hold on
plot(t(decouple)*1e6,I1(decouple), 'x','color', [1 0 0])
plot(t*1e6,I1,'color', [0 0 1])
title('Coil Current 1')
xlabel('t [\mus]')
ylabel('I_1 [A]')

figure('name','Plasma Current 2','outerposition',[xx-1*figdim
     yy-2*figdim figdim figdim])
hold on
```

```
265 plot(t(decouple)*1e6,I2(decouple), 'x','color', [1 0 0])
266 plot(t*1e6,I2,'color', [0 0 1])
267 title('Plasma Current 2')
268 xlabel('t [\mus]')
269 ylabel('I_2 [A]')
270
271 figure('name','Entrained Mass','outerposition',[xx-3.5*figdim
        yy-2.5*figdim figdim figdim])
272 hold on
273 plot(t(decouple)*1e6,m(decouple), 'x','color', [1 0 0])
274 plot(t*1e6,m,'color', [0 0 1])
275 title('Entrained Mass')
276 xlabel('t [\mus]')
277 ylabel('m_e_n_t [kg]')
278 axis([0 t(decouple)*2e6 0 1.2*m(decouple)])
279
280 figure('name','z/z0','outerposition',[xx-2.5*figdim yy-2.5*
      figdim figdim figdim])
281 hold on
282 plot(t(decouple)*1e6,z_z0(decouple), 'x','color', [1 0 0])
283 plot(t*1e6,z./z0,'color', [0 0 1])
284 title('Decoupling Ratio z/z_0')
285 xlabel('t [\mus]')
286 ylabel('z/z_0 [-]')
287 axis([0 t(decouple)*2e6 0 2*z_z0(decouple)])
288
289 figure('name','Energy Balance','outerposition',[xx-1.5*figdim
        yy-2.5*figdim figdim figdim])
290 hold on
291 plot(t(decouple)*1e6,E_flow(decouple), 'x','color', [1 0 0],'
      DisplayName','Decoupling Point')
292 plot(t*1e6,E_flow,'color', [0 0 1],'DisplayName','Flow Energy
      ')
293 plot(t*1e6,E1,'color',[1 0 1], 'DisplayName','Coil Energy')
294 % plot(t*1e6,E2,'color',[0 1 1], 'DisplayName','Plasma Energy
      ')
295 plot([0 t(end)*1e6],[E0 E0],'color',[0 1 0],'linewidth',1,'
      DisplayName','Total Energy')
296 title('Energy Balance')
297 xlabel('t [\mus]')
298 ylabel('E1 [J]')
299 axis([0 t(decouple)*2e6 0 2*E_flow(decouple)])
300 legend('location','northwest')
301
302 end
```